bioRxiv preprint doi: https://doi.org/10.1101/843425; this version posted November 15, 2019. The copyright holder for this preprint (which was not certified by peer review) is the author/funder. All rights reserved. No reuse allowed without permission.

Cerebrovascular reactivity assessment with O_2-CO_2 exchange ratio under brief breath hold challenge

Suk Tak Chan[1*], Karleyton C. Evans[2], Tian Yue Song[1], Juliett Selb[1], Andre van der Kouwe[1], Bruce R. Rosen[1], Yong Ping Zheng[3], Andrew Ahn[1], Kenneth K. Kwong[1]

[1] Athinoula A. Martinos Center for Biomedical Imaging, Department of Radiology, Massachusetts General Hospital, Charlestown, Massachusetts, United States of America

[2] Biogen Inc., Cambridge, Massachusetts, United States of America

[3] Department of Biomedical Engineering, The Hong Kong Polytechnic University, Hong Kong Special Administrative Region, China

* Corresponding author

E-mail: phoebe@nmr.mgh.harvard.edu (STC)

Running headline: CVR assessment with O_2-CO_2 exchange ratio under breath holding challenge

bioRxiv preprint doi: https://doi.org/10.1101/843425; this version posted November 15, 2019. The copyright holder for this preprint (which was not certified by peer review) is the author/funder. All rights reserved. No reuse allowed without permission.

Abstract

Hypercapnia during breath holding is believed to be the dominant driver behind the modulation of cerebral blood flow (CBF). Here we showed that the cerebrovascular responses to brief breath hold epochs were coupled not only with increased partial pressure of carbon dioxide (PCO_2), but also with a decrease in partial pressure of oxygen (PO_2). We used transcranial Doppler ultrasound to evaluate the CBF changes during breath holding by measuring the cerebral blood flow velocity (CBFv) in the middle cerebral arteries, a pair of cerebral arteries that supply most parts of the brain. The regional CBF changes during breath hold epochs were mapped with blood oxygenation level dependent (BOLD) signal changes as surrogate of CBF changes using functional magnetic resonance imaging (fMRI) technique. Given the interdependence of the dynamic changes between PCO_2 and PO_2, we found that the breath-by-breath O_2-CO_2 exchange ratio (bER), namely the ratio of changes in PO_2 (ΔPO_2) to changes in PCO_2 (ΔPCO_2) between end inspiration and end expiration, was superior to either ΔPO_2 or ΔPCO_2 alone in coupling with the changes of CBFv and BOLD signals under breath hold challenge. The regional cerebrovascular reactivity (CVR) results derived by regressing BOLD signal changes on bER under breath hold challenge resembled those derived by regressing BOLD signal changes on end-tidal partial pressure of CO_2 ($P_{ET}CO_2$) under exogenous CO_2 challenge. Our findings provide a novel insight on

bioRxiv preprint doi: https://doi.org/10.1101/843425; this version posted November 15, 2019. The copyright holder for this preprint (which was not certified by peer review) is the author/funder. All rights reserved. No reuse allowed without permission.

the potential of using bER to better quantify CVR changes under breath hold challenge, although the physiological mechanisms of cerebrovascular changes underlying breath hold and exogenous CO_2 challenges are potentially different.

bioRxiv preprint doi: https://doi.org/10.1101/843425; this version posted November 15, 2019. The copyright holder for this preprint (which was not certified by peer review) is the author/funder. All rights reserved. No reuse allowed without permission.

Introduction

Breath hold challenge has been used in the clinical setting as a simple vasoactive stimulus for the assessment of cerebrovascular reactivity (CVR) [1, 2] in patients with carotid artery diseases [3-5] as well as brain tumors [6]. Its use for CVR assessment with transcranial Doppler sonography (TCD) measurement was first demonstrated by Ratnatunga and Adiseshiah [3]. The cerebral blood flow velocities (CBFv) were often measured in the middle cerebral arteries which supply most parts of the brain. The time of breaths (ToB) had often been taken as an indicator of the strength of the vasoactive stimulus to induce changes of cerebral blood flow (CBF). The ratio of CBF to ToB was known as a breath hold index to evaluate CVR [1, 2, 4, 5, 7]. Although TCD offers high temporal resolution to evaluate cerebrovascular responses without the concern of aliasing high frequency hemodynamic signal into the low frequency range, it does not provide regional information. Therefore regional CVR mapping with blood oxygen level-dependent (BOLD) signal changes measured by functional magnetic resonance imaging (fMRI) was used. BOLD-fMRI was used instead of arterial spin labeling (ASL) in MRI perfusion studies due to the low contrast to noise ratio and the low temporal resolution of the ASL technique [8]. ASL image acquisition at a temporal resolution of 4 seconds will under-sample the brain responses within respiratory cycle of 4-6 seconds.

bioRxiv preprint doi: https://doi.org/10.1101/843425; this version posted November 15, 2019. The copyright holder for this preprint (which was not certified by peer review) is the author/funder. All rights reserved. No reuse allowed without permission.

Increased accumulation of carbon dioxide (CO_2) in the blood stream during breath holding had always been considered to be the main vasoactive stimulus [9], and increased end-tidal partial pressure of CO_2 ($P_{ET}CO_2$) was commonly measured as a surrogate for the increased arterial CO_2 level to evaluate CVR [10-12]. Instead of being considered as only a hypercapnic challenge, breath hold can also be recognized as a form of brief hypoxia with concurrent mild hypercapnia [13-15]. We hypothesized that hypoxia and hypercapnia work synergistically to enhance CBF response to breath hold. Hypoxia or changes of end-tidal partial pressure of O_2 ($P_{ET}O_2$) were seldom used to account for CBF changes during breath holding partly due to the common belief that the vasodilatory effect of decreased PO_2 in blood was small. Such a belief stemmed from high altitude studies and lab-controlled low oxygen environment reporting that significant CBF changes only happened in hypoxia with arterial PO_2 (PaO_2) going down to approximately 50 mmHg [16-18]. It should be noted that reports of large CBF increase in response to strong hypoxia were often accompanied by hypocapnia due to hyperventilation in the studies of either high altitudes or lab-controlled low oxygen environment (~8-13% O_2) [16-18]. The case is different with breath hold because hypoxia is accompanied by hypercapnia and not by hypocapnia during breath holding.

bioRxiv preprint doi: https://doi.org/10.1101/843425; this version posted November 15, 2019. The copyright holder for this preprint (which was not certified by peer review) is the author/funder. All rights reserved. No reuse allowed without permission.

In spontaneous breathing, blood gas levels of O_2 and CO_2 are optimized by the feedback control of ventilation via chemoreflexes [19] to regulate blood flow and oxygen delivery to the brain as part of a vital homeostatic process [20]. The feedback loops include interaction between central chemoreceptors at the brainstem [21, 22] and peripheral chemoreceptors at the carotid body [23, 24]. While most of the studies on the role of PO_2 to stimulate peripheral chemoreceptors at the carotid body had been focused on hypoxia [20] where chemoreceptor activities rose quickly in a hyperbolic fashion, Biscoe et al. [25] showed that peripheral chemoreceptor activities could be observed from normoxia to hyperoxia up to arterial PO_2 level of 190mmHg and beyond. Lahiri et al. [26] reported that the stimulus thresholds of arterial PO_2 and PCO_2 for peripheral chemoreceptors were largely interdependent under the normoxic condition where a drop in arterial PO_2 was routinely accompanied by increased chemoreceptor activities as well as an enhanced sensitivity of carotid chemoreceptors to arterial PCO_2. Multiple authors [20, 25-28] reported similar findings for normoxic as well as hypoxic conditions. Ventilation, like chemoreceptors, also becomes more sensitive to PCO_2 with a slight decrease in PO_2 within the range of normoxia (90-110 mmHg). The same interaction between change in PO_2 and change in peripheral chemoreceptor activities during spontaneous breathing is also assumed to take place during breath hold. In terms of the relationship between modulated

bioRxiv preprint doi: https://doi.org/10.1101/843425; this version posted November 15, 2019. The copyright holder for this preprint (which was not certified by peer review) is the author/funder. All rights reserved. No reuse allowed without permission.

chemoreceptor activities and cerebral hemodynamic responses, previous studies reported that apnea-induced hypoxia and hypercapnia caused chemoreceptor-mediated central vasodilation and concurrent peripheral vasoconstriction to conserve oxygen delivery to the brain [15], leading to an increase in cerebral blood flow (CBF) and a decrease in peripheral oxygen saturation [29]. The detailed mechanisms to link change in chemoreceptor activities and change in CBF remain to be a topic of on-going research. We proposed to examine breath hold in the framework of mild hypoxia and mild hypercapnia based on the findings on hemodynamic responses to hypoxia with maintained eucapnia or in the presence of hypercapnia in humans reported by Shapiro et al. [30] and Mardimae et al. [31]. Small and progressive increase in CBF was indeed observed in small steps of serial reductions of PO_2 starting from normoxia with maintained eucapnia [30] as well as with slight hypercapnia of around 45 mmHg [31]. The findings in these studies suggested that mild hypercapnia could increase the sensitivity of the CBF response to a very mild level of hypoxia and the ranges of mild PO_2 and PCO_2 changes reported are achievable by breath hold. We therefore hypothesized that mild hypoxia and mild hypercapnia in breath hold could work synergistically to enhance CBF response.

In the current study, we hypothesized that the change of PCO_2 and of PO_2, while interdependent, were not necessarily redundant in terms of their temporal and frequency

bioRxiv preprint doi: https://doi.org/10.1101/843425; this version posted November 15, 2019. The copyright holder for this preprint (which was not certified by peer review) is the author/funder. All rights reserved. No reuse allowed without permission.

characteristics. Our hypothesis differs from the belief that the changes of PCO_2 and of PO_2 in respiration are just mirror image of each other. We further hypothesized that change of PO_2 and of PCO_2 were different from each other in their coherence with cerebral hemodynamic signal changes under breath hold challenge. During breath holding, the alveolar gas is not refreshed by the ambient air and it creates a brief period of mild hypoxia with concurrent mild hypercapnia. While question of collinearity often comes up when interdependent changes of PCO_2 and PO_2 are included as predictor variables in the same regression model of CVR quantification, the interdependence between changes of PO_2 (ΔPO_2) and PCO_2 (ΔPCO_2) can be more naturally characterized by their breath-by breath exchange ratio ($\Delta PO_2/\Delta PCO_2$), namely bER. We hypothesized that bER would be able to better characterize CVR under breath hold challenge in the regression model without creating a problem of collinearity.

We preferred the terms ΔPO_2 (expired PCO_2 – inspired PCO_2) and ΔPCO_2 (inspired PO_2 – expired PO_2) over the more commonly used $P_{ET}O_2$ and $P_{ET}CO_2$ because the breath-by-breath ΔPO_2 and ΔPCO_2 are related to the partial pressure of systemic O_2 uptake and CO_2 release respectively. bER takes advantage of its ratio format to reduce the unwanted effects of ventilatory volume fluctuations due to isolated deep breaths common to ΔPO_2 and ΔPCO_2 measured. bER is mathematically equivalent to the *reciprocal* of the

bioRxiv preprint doi: https://doi.org/10.1101/843425; this version posted November 15, 2019. The copyright holder for this preprint (which was not certified by peer review) is the author/funder. All rights reserved. No reuse allowed without permission.

respiratory exchange ratio (RER) from alveolar gas equation [32], except that bER is a dynamic breath-by-breath measurement and RER is a steady-state time-averaged measurement over a period of time. RER has been used to evaluate resting systemic metabolic rate [33-35]. However, some technical differences need to be mentioned between RER used in the literature and bER we used in this study. Traditionally, RER is derived by measuring the respiratory flow and the expired gases collected in Douglas bag connected to a closed circuit over several minutes. bER is derived here by measuring the inspired and expired gases with a nasal tubing at each breath.

In this study, the primary objective was to evaluate our hypothesis that bER would be a more useful index than $P_{ET}CO_2$ to correlate with the changes of CBFv and BOLD signals in the evaluation of cerebral hemodynamic responses to the breath hold challenge. To address the question of redundancy among respiratory gas exchange (RGE) metrics, we examined the correlations among bER, ΔPCO_2, ΔPO_2, $P_{ET}CO_2$, $P_{ET}O_2$ and ToB in both TCD and MRI sessions. In the first part of the study, we correlated the time series of the RGE metrics (bER, ΔPCO_2, ΔPO_2 and ToB) with those of CBFv and BOLD signal changes under the protocol of breath hold challenge. We then examined the temporal features and frequency characteristics of these RGE metrics as well as their coherence with CBFv and BOLD signal changes. In the second part of the study, we compared the regional CVR

bioRxiv preprint doi: https://doi.org/10.1101/843425; this version posted November 15, 2019. The copyright holder for this preprint (which was not certified by peer review) is the author/funder. All rights reserved. No reuse allowed without permission.

maps obtained by regressing BOLD signal changes on selected RGE metrics including bER, $P_{ET}CO_2$ and ToB under breath hold challenge with regional CVR maps obtained by regressing BOLD signals changes on $P_{ET}CO_2$ obtained under exogenous CO_2 hypercapnic challenge. The success of such association between bER and cerebral hemodynamic responses, in addition to offering a better physiological model to characterize cerebral hemodynamic responses under breath hold challenge, would also provide a novel insight in the study of brain-body interaction.

bioRxiv preprint doi: https://doi.org/10.1101/843425; this version posted November 15, 2019. The copyright holder for this preprint (which was not certified by peer review) is the author/funder. All rights reserved. No reuse allowed without permission.

Materials and Methods

Participants

Seventeen volunteers aged from 22 to 48 years (mean=31.18 years; SD=8.78 years; 11M and 6F) were included. All of them were recruited by e-mail and poster placement within the Partners hospital network. They were screened to exclude neurological, mental and medical disorders and drug abuse. TCD and MRI scanning were performed in the Athinoula A. Martinos Center for Biomedical Imaging at the Massachusetts General Hospital of Partners HealthCare. All the experimental procedures were explained to the subjects, and signed informed consent was obtained prior to participation in the study. All components of this study were performed in compliance with the Declaration of Helsinki and all procedures were approved by Partners Human Research Committee.

Our study was divided into Part 1 and Part 2. In Part 1, we aimed to correlate the RGE metrics including bER, ΔPO_2, ΔPCO_2 and ToB with cerebral hemodynamic responses including CBFv and BOLD signal changes to breath hold challenge. We also examined the temporal features and frequency characteristics of RGE metrics and their coherence with cerebral hemodynamic responses. Sixteen out of 17 subjects performed breath hold tasks in the MRI sessions, while 12 of them participated in TCD sessions. In Part 2, we aimed to

bioRxiv preprint doi: https://doi.org/10.1101/843425; this version posted November 15, 2019. The copyright holder for this preprint (which was not certified by peer review) is the author/funder. All rights reserved. No reuse allowed without permission.

assess the usefulness of bER in the regional breath hold CVR quantification by comparing the regional CVR maps obtained by regressing BOLD signal changes on bER, $P_{ET}CO_2$ and ToB under breath hold challenge with regional CVR maps obtained by regressing BOLD signals changes on $P_{ET}CO_2$ under exogenous CO_2 challenge. Ten out of 17 subjects had additional exogenous CO_2 challenge for comparison. Before we correlated the changes of RGE metrics with CBFv and BOLD signal changes under breath hold challenge, we examined the correlations among the RGE metrics (bER, ΔPCO_2, ΔPO_2, $P_{ET}CO_2$, $P_{ET}O_2$ and ToB) acquired in both TCD and MRI sessions.

Part 1: Breath hold challenge

Transcranial Doppler scanning

Before the study of blood flow velocity in intracranial arteries, subject was allowed to rest at least 20-30 minutes for hemodynamic stabilization. The blood pressure measured in the subject was within the normal range [36]. With the subject in a sitting position, a dual probe setting with 2MHz transducers in conjunction with TCD system (Delicate EMS-9U, Shenzhen, China) was used for simultaneous recording of CBFv in the middle cerebral arteries (MCA) on both left and right sides while the subject was performing the breath

bioRxiv preprint doi: https://doi.org/10.1101/843425; this version posted November 15, 2019. The copyright holder for this preprint (which was not certified by peer review) is the author/funder. All rights reserved. No reuse allowed without permission.

hold task. Two transducers were attached onto the left and right temporal bone window by velcro. The depth of the Doppler samples was confined to the M1 segment, which is at the main stem of the MCA, for all the subjects.

The timing of the breath hold task was presented visually to the subject by a computer using the software Eprime Professional 2.0 (Psychology Software Tools, Inc., Pittsburgh, USA). A rehearsal session was given to each subject to practice breath hold task. Each subject was instructed via visual cues to perform 6 epochs of 30-second breath hold interleaved with 60-90 seconds of free breathing (Fig 1). They were instructed by visual cues to only hold their breath for as long as they could during the 30-second period. Multiple epochs of breath holding followed by free breathing increased the samples for quantitative analysis. The total duration of the breath hold protocol lasted 10 minutes.

Fig 1. Paradigms of (A) breath hold and (B) exogenous CO_2 challenges. The timing for the onset and the end of breath hold epochs is the same as that for exogenous CO_2 hypercapnic epochs. The duration of normal breathing phases in breath hold challenge and normocapnic phases in exogenous CO_2 challenge varies from 60 seconds to 90 seconds.

bioRxiv preprint doi: https://doi.org/10.1101/843425; this version posted November 15, 2019. The copyright holder for this preprint (which was not certified by peer review) is the author/funder. All rights reserved. No reuse allowed without permission.

Physiological changes including PCO_2, PO_2, electrocardiogram (ECG) and peripheral blood pressure were measured simultaneously with TCD acquisition. A small nasal tubing was placed at the subject's nostril to sample PCO_2 and PO_2 via gas analyzers (Capstar-100, Oxystar-100, CWE, Inc., PA, USA) after calibrating to the barometric pressure of the day of TCD scanning and correcting for vapor pressure. Peripheral blood pressure was continuously measured with Finometer MIDI (Finapres Medical Systems B.V., Netherlands). All the TCD and physiological measurements were synchronized using trigger signals from E-prime. CBFv time series and physiological recordings were stored for offline data analysis.

MRI acquisition

MRI brain scanning was performed on a 3-Tesla scanner (Siemens Medical, Erlangen, Germany). The head was immobilized in a standard head coil with foam pads. The following whole brain MRI datasets were acquired on each subject: 1) standard high-resolution sagittal images acquired with volumetric T1-weighted 3D-MEMPRAGE sequence (TR=2530ms, TE=1.74ms/3.6ms/5.46ms/7.32ms, flip angle=7º, FOV=256×256mm, matrix=256×256, slice thickness=1mm); 2) BOLD-fMRI images acquired with gradient-echo echo planar imaging (EPI) sequence (TR=1450ms, TE=30ms,

bioRxiv preprint doi: https://doi.org/10.1101/843425; this version posted November 15, 2019. The copyright holder for this preprint (which was not certified by peer review) is the author/funder. All rights reserved. No reuse allowed without permission.

flip angle=90º, FOV=220×220mm, matrix=64×64, slice thickness=5mm, slice gap=1mm) while the subject was performing the breath hold task. The breath hold task and the physiological set-up used for gas sampling in MRI session were the same as those used in TCD sessions. The gas analyzers were again calibrated to the barometric pressure of the day of MRI scanning and corrected for vapor pressure. ECG was measured using Siemens physiological monitoring unit. Physiological changes including PCO_2, PO_2 and ECG were measured simultaneously with MRI acquisition. All the physiological measurements were synchronized using trigger signals from the MRI scanner. BOLD-fMRI images and physiological recordings were stored for offline data analysis.

Part 2: Exogenous CO_2 challenge

Ten out of 16 subjects had additional exogenous CO_2 challenge in the MRI session. Given that there is significant inter-individual variance in resting $P_{ET}CO_2$ [37], resting $P_{ET}CO_2$ was assessed in those subject via calibrated capnograph before the exogenous CO_2 challenge. Subject wore nose-clip and breathed through a mouth-piece on an MRI-compatible circuit designed to maintain the $P_{ET}CO_2$ within ± 1-2 mmHg of target $P_{ET}CO_2$ [38, 39]. The fraction of inspired carbon dioxide was adjusted to produce steady-state

bioRxiv preprint doi: https://doi.org/10.1101/843425; this version posted November 15, 2019. The copyright holder for this preprint (which was not certified by peer review) is the author/funder. All rights reserved. No reuse allowed without permission.

conditions of normocapnia and mild hypercapnia (4-8 mmHg above the subject's resting $P_{ET}CO_2$). The CO_2 challenge paradigm consisted of 2 consecutive phases (normocapnia and mild hypercapnia) repeating 6 times with 3 epochs of 4 mmHg increase and 3 epochs of 8 mmHg increase of $P_{ET}CO_2$ (Fig 1). The normocapnia phase lasted 60-90 seconds, while the mild hypercapnia phase lasted 30 seconds. The total duration of the exogenous CO_2 hypercapnic challenge lasted 10 minutes.

When the subject had exogenous CO_2 challenge in MRI session, BOLD-fMRI images were acquired using the same EPI sequence for breath hold challenge. The PCO_2 and PO_2 were sampled through the air filter connected with the mouthpiece and the sampled gases were measured by calibrated gas analyzers. The respiratory flow was measured with respiratory flow head (MTL300L, AdInstruments, Inc., CO, USA) on the breathing circuit via calibrated spirometer (FE141, AdInstruments, Inc., CO, USA). The physiological measurements were synchronized with MRI images using trigger signals from MRI scanner. All the BOLD-fMRI images and physiological recordings were stored for offline data analysis.

bioRxiv preprint doi: https://doi.org/10.1101/843425; this version posted November 15, 2019. The copyright holder for this preprint (which was not certified by peer review) is the author/funder. All rights reserved. No reuse allowed without permission.

Data analysis

Processing of physiological data

The physiological data from both TCD and MRI sessions were analyzed using Matlab R2014a (Mathworks, Inc., Natick, MA, USA). Technical delay of PCO_2 and PO_2 was corrected by cross-correlating the time series of PCO_2 and PO_2 with respiratory phases determined from the artifactual displacement due to chest excursion on ECG time series for the breath hold runs in the TCD sessions, with the respiratory phases from the respiratory bellow for the breath hold runs in the MRI sessions, and with the respiratory flow for the exogenous CO_2 runs.

End inspiration (I) and end expiration (E) were defined on the time series of PO_2 and PCO_2 (S1 Fig). They were verified by the inspiratory and expiratory phases on the respiration time series. The breath-by-breath end-tidal CO_2 ($P_{ET}CO_2$) and end-tidal O_2 ($P_{ET}O_2$) were extracted at the end expiration of PCO_2 and PO_2 time series respectively. Changes of the gas parameters during breath hold periods were interpolated by the values measured immediately before and after the breath hold periods. The duration of breathing cycle, which is known as time of breath (ToB), was derived by subtracting the timing in seconds of the 2 consecutive end expiration markers. Breath-by-breath O_2-CO_2 exchange

bioRxiv preprint doi: https://doi.org/10.1101/843425; this version posted November 15, 2019. The copyright holder for this preprint (which was not certified by peer review) is the author/funder. All rights reserved. No reuse allowed without permission.

ratio (bER) is defined as the ratio of the change in PO_2 (ΔPO_2 = inspired PO_2 – expired PO_2) to the change in PCO_2 (ΔPCO_2 = expired PCO_2 – inspired PCO_2) measured between end inspiration and end expiration in each respiratory cycle.

Simple correlation analyses were applied on the time series of RGE metrics (bER, ΔPCO_2, ΔPO_2, $P_{ET}CO_2$, $P_{ET}O_2$ and ToB) in pairs, which were acquired in both TCD and MRI sessions. Time series of the RGE metrics including bER, ΔPO_2, ΔPCO_2 and ToB were also used in the CBFv and BOLD data analyses.

Preprocessing of CBFv data

The CBFv data were analyzed using Matlab R2014a (Mathworks, Inc., Natick, MA, USA). A median filter was applied to the data to reduce artifactual spikes. Beat-by-beat systolic peaks and end-diastolic troughs were determined using custom Matlab function and corrected on the graphical user interface incorporated in the function. Systolic peaks and end-diastolic troughs of cardiac cycles on the CBFv time series showing persistent artifacts were excluded in the following analysis. TCD data in both left and right MCAs were acquired on 12 subjects. One of the 12 TCD datasets had persistent artifacts in over one-third of the time series acquired in the LMCA. The CBFv time series in the LMCA of that

bioRxiv preprint doi: https://doi.org/10.1101/843425; this version posted November 15, 2019. The copyright holder for this preprint (which was not certified by peer review) is the author/funder. All rights reserved. No reuse allowed without permission.

particular TCD dataset was excluded in further analysis. Time series of mean CBFv was derived by integrating the CBFv over each cardiac cycle. In order to reduce the large inter-individual variations of absolute blood flow velocities [40, 41] and to remove the dependence of insonation angle [42], the percent change of CBFv (ΔCBFv) of the left and right MCAs relative to baseline value was derived. The mean CBFv for a period of 30 seconds at the beginning of the time series was chosen as the baseline because the subject was in resting state and the CBFv acquired within this period had the least effect from the respiratory challenges.

Preprocessing of BOLD-fMRI data

All the BOLD-fMRI data were imported into the software Analysis of Functional NeuroImage (AFNI) [43] (National Institute of Mental Health, http://afni.nimh.nih.gov) for time-shift correction, motion correction, normalization and detrending. The first 12 volumes in the first 12 time points of each functional dataset, collected before equilibrium magnetization was reached, were discarded. Each functional dataset was corrected for slice timing, motion-corrected and co-registered to the first image of the first functional dataset using three-dimensional volume registration. It was then normalized to its mean intensity

bioRxiv preprint doi: https://doi.org/10.1101/843425; this version posted November 15, 2019. The copyright holder for this preprint (which was not certified by peer review) is the author/funder. All rights reserved. No reuse allowed without permission.

value across the time-series. Voxels located within the ventricles and outside the brain defined in the parcellated brain volume using FreeSurfer [44] (MGH/MIT/HMS Athinoula A. Martinos Center for Biomedial Imaging, Boston, http://surfer.nmr.mgh.harvard.edu) were excluded from the following analyses of functional images. The time-series of each voxel in the normalized functional dataset was detrended with the 5^{th} order of polynomials to remove the low drift frequency. Individual brain volumes with time series of percent BOLD signal changes (ΔBOLD) were derived.

Part 1:

Correlation analysis between cerebral hemodynamic responses and RGE metrics

The cerebral hemodynamic responses (ΔCBFv and ΔBOLD) were separately correlated with the RGE metrics including bER, ΔPCO_2, ΔPO_2 and ToB. The correlation indicated by Pearson's correlation coefficient was considered significant at $p<0.05$. Fisher Z-transformation was used to transform Pearson's correlation coefficients to Fisher Z scores for group analysis. Paired t-tests were used to compare the Fisher Z scores representing the correlation between cerebral hemodynamic responses and bER with those

bioRxiv preprint doi: https://doi.org/10.1101/843425; this version posted November 15, 2019. The copyright holder for this preprint (which was not certified by peer review) is the author/funder. All rights reserved. No reuse allowed without permission.

indicating the correlation between cerebral hemodynamic responses and RGE metrics other than bER. Differences were considered to be significant at $p<0.05$.

Dynamic analysis of coherence between cerebral hemodynamic responses and RGE metrics as function of time and frequency

Wavelet transform coherence is a method for analyzing the coherence and phase lag between two time series as a function of both time and frequency [45-47]. It is therefore well suited to investigating non-stationary changes in coupling between the time series of cerebral hemodynamic responses (ΔCBFv and ΔBOLD) and the time series of RGE metrics including bER, ΔPCO_2, ΔPO_2 and ToB, as well as the phase lag of the cerebral hemodynamic responses to each of the metrics. The time series of ΔBOLD were extracted from left gray matter (LGM), right gray matter (RGM), left white matter (LWM) and right white matter (RWM). We used the Matlab wavelet cross-spectrum toolbox developed by Grinsted et al. [46]. Squared wavelet coherence between time series of RGE metrics and cerebral hemodynamic responses (ΔCBFv and ΔBOLD) was separately plotted with x-axis as time and y-axis as scale which had been converted to its equivalent Fourier period. An example of squared wavelet coherence between bER and ΔCBFv in right MCA from a

bioRxiv preprint doi: https://doi.org/10.1101/843425; this version posted November 15, 2019. The copyright holder for this preprint (which was not certified by peer review) is the author/funder. All rights reserved. No reuse allowed without permission.

representative subject under breath hold challenge is shown in S2 Fig. The magnitude of wavelet transform coherence ranged between 0 and 1 that can be conceptualized as a localized correlation coefficient in time and frequency space [46]. The phase angle between the two time series at particular samples of the time-frequency plane is indicated by an arrow: a rightward pointing arrow indicates that the time series are in phase, or positively correlation ($\phi=0$); a leftward pointing arrow indicates anticorrelation ($\phi=\pi$), and the downward and upward pointing arrows indicate phase angles of $\pi/2$ and $-\pi/2$ relative to $\phi=0$, respectively. Areas inside the 'cone of influence', which are locations in the time-frequency plane where edge effects give rise to lower confidence in the computed values, are shown in faded color outside of the conical contour. The statistical significance level of the wavelet coherence is estimated using Monte Carlo method and the 5% significance level against red noise is shown as thick contour in the squared wavelet coherence plot. The wavelet coherence magnitudes and phases bounded by thick contour outside the cone of influence are considered significant.

Time-averaged coherence is defined as the total significant coherence at each scale of Fourier periods (converted into frequency) where the wavelet coherence magnitude exceeds 95% significance level, normalized by the maximum possible coherence outside the cone of influence at that particular scale (S2 Fig). It is interpreted in the similar way as

bioRxiv preprint doi: https://doi.org/10.1101/843425; this version posted November 15, 2019. The copyright holder for this preprint (which was not certified by peer review) is the author/funder. All rights reserved. No reuse allowed without permission.

the coherence in the transfer function analysis which has been used in cerebral autoregulation study [48]. The mean time-averaged coherence at the phase lags of $0\pm\pi/2$ and $\pi\pm\pi/2$ were plotted for all subjects included in TCD or MRI sessions to explore the Fourier periods/frequency bandwidths that oscillations of cerebral hemodynamic responses (ΔCBFv and ΔBOLD) were in synchrony with each physiological time series of bER, ΔPO_2, ΔPCO_2 and ToB when the subjects were performing breath hold task.

Part 2:

Linear regression for CVR quantification

Linear regression analysis was used to derive CVR from the time series of ΔBOLD and vasoactive stimulus when the subject was under breath hold and exogenous CO_2 challenges. The time series of each of the commonly used vasoactive stimuli (bER, $P_{ET}CO_2$ and ToB) served as a regressor in a separate linear regression analysis. CVR was defined as the percent BOLD signal changes per unit change of the vasoactive stimulus. Therefore CVR was quantified by the coefficient of regression, i.e. the slope.

The statistical parametric maps for individual subjects were cluster-corrected using a threshold estimated with Monte Carlo simulation algorithm. Individual subject brain

bioRxiv preprint doi: https://doi.org/10.1101/843425; this version posted November 15, 2019. The copyright holder for this preprint (which was not certified by peer review) is the author/funder. All rights reserved. No reuse allowed without permission.

volume with CVR magnitude was registered onto each subject's anatomical scan and transformed to the standardized space of Talairach and Tournoux [49]. In order to protect against type I error, individual voxel probability threshold of $p<0.005$ was held to correct the overall significance level to $\alpha<0.05$. Monte Carlo simulation was used to correct for multiple comparisons [50]. Based upon a Monte Carlo simulation with 2000 iteration processed with ClustSim program [51], it was estimated that a 476mm^3 contiguous volume would provide the significance level $\alpha<0.05$, which met the overall corrected threshold of $p<0.05$.

Group comparison of CVR between breath hold and exogenous CO_2 challenges

For each subject who participated in both breath hold and exogenous CO_2 MRI scanning, CVR values were derived from regressing ΔBOLD on bER ($CVR_{BH\text{-}bER}$), ΔBOLD on $P_{ET}CO_2$ ($CVR_{BH\text{-}PETCO2}$) and ΔBOLD on ToB ($CVR_{BH\text{-}ToB}$) when the subjects were under breath hold challenge. $CVR_{BH\text{-}bER}$, $CVR_{BH\text{-}PETCO2}$ and $CVR_{BH\text{-}ToB}$ values were separately averaged in each of the 160 brain regions parcellated by the software FreeSurfer. Using the same method, CVR values during exogenous CO_2 challenge were obtained by

bioRxiv preprint doi: https://doi.org/10.1101/843425; this version posted November 15, 2019. The copyright holder for this preprint (which was not certified by peer review) is the author/funder. All rights reserved. No reuse allowed without permission.

regressing ΔBOLD on $P_{ET}CO_2$ ($CVR_{CO2\text{-}PETCO2}$). $CVR_{CO2\text{-}PETCO2}$ values were averaged in each of the 160 brain regions. To study the CVR changes in group, one-sample t-tests were applied onto the brain volumes with regional $CVR_{BH\text{-}bER}$, $CVR_{BH\text{-}PETCO2}$, $CVR_{BH\text{-}ToB}$ and $CVR_{CO2\text{-}PETCO2}$. Differences were considered significant at false discovery rate adjusted $p_{fdr}<0.05$.

The physiological mechanisms underlying breath holding and exogenous CO_2 hypercapnia are potentially different. To study the precision of vasoactive stimulus in predicting the regional cerebral hemodynamic responses, percentage of voxels in each region having significant CVR changes that survived at cluster-corrected $p<0.05$ in individual subject analysis, in short vCVR, were calculated. Individual subject brain volumes with regional vCVR due to $P_{ET}CO_2$, ($vCVR_{BH\text{-}PETCO2}$), ToB ($vCVR_{BH\text{-}ToB}$) and bER ($vCVR_{BH\text{-}bER}$) were obtained in breath hold MRI scanning, while those with regional vCVR due to $P_{ET}CO_2$ ($vCVR_{CO2\text{-}PETCO2}$) were obtained in exogenous CO_2 MRI scanning. One sample t-tests were again applied for group analysis. Differences were considered significant at $p_{fdr}<0.05$.

To study the usefulness of $P_{ET}CO_2$, ToB and bER in CVR quantification under breath hold challenge, using $vCVR_{CO2\text{-}PETCO2}$ as reference, paired t-tests were applied to compare the regional brain maps of $vCVR_{CO2\text{-}PETCO2}$ under exogenous CO_2 challenge with

bioRxiv preprint doi: https://doi.org/10.1101/843425; this version posted November 15, 2019. The copyright holder for this preprint (which was not certified by peer review) is the author/funder. All rights reserved. No reuse allowed without permission.

those of $vCVR_{BH\text{-}PETCO2}$, $vCVR_{BH\text{-}ToB}$ and $vCVR_{BH\text{-}bER}$ in groups. Differences were considered significant at $p_{fdr}<0.05$.

bioRxiv preprint doi: https://doi.org/10.1101/843425; this version posted November 15, 2019. The copyright holder for this preprint (which was not certified by peer review) is the author/funder. All rights reserved. No reuse allowed without permission.

Results

Part 1:

Subject demographics were shown in Table 1. The $P_{ET}CO_2$, $P_{ET}O_2$, ΔPCO_2, ΔPO_2 and bER measured in the baseline periods, i.e. the period before the first breath hold epoch, in the TCD and MRI sessions were summarized in Tables 2A and 2B respectively. The breath hold duration, the changes of ΔPCO_2, ΔPO_2, bER, ΔCBFv and ΔBOLD averaged over the 6 breath hold epochs from the onset to the end of each breath hold epoch were also included. Most of the subjects were able to hold their breaths for 30 seconds on average. The averaged changes of ΔPO_2 from the onset to the end of the breath hold epochs were almost 3 to 4 folds larger than those of ΔPCO_2.

Table 1. Subject demographics and their participation in breath hold and exogenous CO_2 challenges in the TCD and MRI sessions.

			TCD	MRI	
Subjects	**Gender**	**Age**	**Breath Hold Challenge**	**Breath Hold Challenge**	**Exogenous CO2 Challenge**
s1	M	35	-	√	√
s2	M	48	-	√	√
s3	M	22	-	√	√
s4	M	38	√	√	√
s5	M	28	√	√	-
s6	M	27	√	√	√
s7	M	32	√	√	√
s8	M	22	√	√	√
s9	M	32	√	√	√
s10	F	26	√	√	√
s11	F	27	√	√	√
s12	F	47	√	√	-
s13	M	46	-	√	-
s14	F	25	√	√	-
s15	F	23	√	√	-
s16	M	29	-	√	-
s17	F	23	√	-	-
Number of subjects:			12	16	10

Table 2A. RGE metrics and ΔCBFv in TCD sessions.

	Baseline					**Averaged Changes From the Onset to the End of Breath Hold Epochs**					
Subjects	**$P_{ET}CO_2$ (mmHg)**	**$P_{ET}O_2$ (mmHg)**	**ΔPCO_2 (mmHg)**	**ΔPO_2 (mmHg)**	**bER**	**Breath Hold Duration (seconds)**	**ΔPCO_2 (mmHg)**	**ΔPO_2 (mmHg)**	**bER**	**ΔCBFv in LMCA (%)**	**ΔCBFv in RMCA (%)**
s4	39.6 (0.5)	108.5 (0.6)	39.7 (0.5)	42.7 (0.6)	1.1 (0.0)	30.7 (1.3)	8.9 (7.7)	25.1 (14.2)	0.4 (0.1)	43.4 (9.2)	43.4 (9.1)
s5	39.5 (1.7)	112.0 (2.5)	37.3 (4.4)	44.6 (5.4)	1.2 (0.0)	35.5 (0.6)	3.4 (0.8)	18.2 (2.4)	0.4 (0.1)	21.1 (4.6)	31.8 (2.7)

bioRxiv preprint doi: https://doi.org/10.1101/843425; this version posted November 15, 2019. The copyright holder for this preprint (which was not certified by peer review) is the author/funder. All rights reserved. No reuse allowed without permission.

s6	34.3 (0.5)	116.5 (0.7)	33.6 (0.5)	32.2 (0.7)	1.0 (0.0)	33.1 (1.4)	7.7 (4.1)	32.2 (9.5)	0.6 (0.1)	37.2 (6.5)	40.5 (10.3)
s7	39.2 (1.0)	102.9 (1.5)	39.3 (1.0)	48.7 (1.7)	1.2 (0.0)	31.7 (2.4)	8.3 (1.5)	38.6 (5.7)	0.7 (0.1)	51.3 (12.6)	46.7 (11.2)
s8	38.3 (0.7)	104.6 (1.2)	37.3 (0.6)	46.4 (1.4)	1.2 (0.0)	33.0 (1.4)	5.6 (3.7)	27.4 (11.4)	0.5 (0.1)	42.5 (7.9)	41.9 (7.4)
s9	34.7 (0.4)	106.4 (0.9)	35.1 (0.4)	45.9 (1.0)	1.3 (0.0)	38.2 (4.4)	2.8 (3.6)	11.4 (17.8)	0.2 (0.3)	28.7 (12.9)	28.6 (8.8)
s10	30.7 (0.8)	116.2 (2.2)	30.6 (0.4)	36.8 (1.8)	1.2 (0.0)	34.1 (1.4)	8.5 (1.0)	39.3 (6.0)	0.8 (0.2)	31.1 (9.0)	32.6 (7.6)
s11	35.6 (0.4)	109.9 (0.7)	35.0 (0.4)	40.3 (0.8)	1.2 (0.0)	32.6 (1.5)	4.7 (1.5)	27.7 (3.1)	0.6 (0.1)	---	39.5 (7.4)
s12	35.3 (0.2)	116.0 (0.5)	34.6 (0.2)	35.0 (0.8)	1.0 (0.0)	32.1 (1.5)	8.7 (1.3)	40.3 (3.0)	0.8 (0.0)	43.6 (2.3)	52.5 (1.7)
s14	33.9 (0.3)	121.2 (0.7)	30.1 (0.5)	32.0 (1.1)	1.1 (0.0)	31.7 (3.8)	3.9 (1.6)	17.5 (2.3)	0.5 (0.1)	51.1 (3.2)	46.1 (5.8)
s15	31.9 (0.8)	118.8 (0.7)	28.3 (1.3)	32.8 (1.2)	1.2 (0.0)	30.6 (2.3)	8.0 (3.9)	27.5 (3.5)	0.7 (0.2)	53.0 (7.0)	50.8 (7.0)
s17	31.9 (2.1)	120.2 (2.8)	27.5 (3.5)	31.3 (4.5)	1.1 (0.0)	23.3 (2.7)	2.5 (3.7)	15.8 (9.8)	0.5 (0.3)	38.9 (9.1)	36.1 (5.7)

Baseline mean values (SD) of $P_{ET}CO_2$, $P_{ET}O_2$, ΔPCO_2, ΔPO_2 and bER for all subjects (n=12) who were under breath hold challenge in the TCD sessions (*left*). The averaged changes (SD) of breath hold duration, ΔPCO_2, ΔPO_2, bER, ΔCBFv measured in LMCA and RMCA from the onset to the end of the breath hold epochs in the TCD sessions (*right*).

Table 2B. RGE metrics and ΔBOLD in MRI sessions.

	Baseline					**Averaged Changes From the Onset to the End of Breath Hold Epochs**							
Subjects	**$P_{ET}CO_2$ (mmHg)**	**$P_{ET}O_2$ (mmHg)**	**ΔPCO_2 (mmHg)**	**ΔPO_2 (mmHg)**	**bER**	**Breath Hold Duration (seconds)**	**ΔPCO_2 (mmHg)**	**ΔPO_2 (mmHg)**	**bER**	**ΔBOLD in LGM (%)**	**ΔBOLD in RGM (%)**	**ΔBOLD in LWM (%)**	**ΔBOLD in RWM (%)**
s1	42.9 (0.7)	99.3 (2.3)	42.5 (0.7)	54.0 (2.8)	1.3 (0.0)	33.4 (3.1)	3.9 (2.4)	29.7 (7.6)	0.6 (0.1)	2.3 (0.6)	2.2 (0.4)	1.0 (0.2)	1.0 (0.2)
s2	38.7 (0.1)	113.8 (0.2)	36.6 (0.6)	32.7 (0.4)	0.9 (0.0)	31.7 (1.4)	9.5 (2.7)	40.5 (2.5)	0.8 (0.1)	2.1 (0.7)	2.2 (0.5)	1.1 (0.2)	1.2 (0.2)
s3	36.1 (0.3)	112.7 (1.1)	35.9 (0.3)	38.1 (1.7)	1.1 (0.0)	32.6 (2.7)	5.3 (1.9)	46.8 (5.3)	1.0 (0.2)	2.3 (1.3)	2.5 (1.6)	1.3 (0.6)	1.3 (0.8)
s4	39.4 (0.7)	104.1 (1.2)	39.2 (0.7)	44.2 (1.5)	1.1 (0.0)	35.5 (1.4)	1.7 (1.3)	17.3 (6.8)	0.4 (0.1)	2.5 (0.4)	3.7 (1.1)	1.3 (0.2)	1.6 (0.6)
s5	32.4 (0.4)	117.1 (0.4)	32.1 (0.4)	32.4 (0.5)	1.0 (0.0)	35.3 (1.3)	7.6 (5.4)	30.9 (6.0)	0.7 (0.1)	1.6 (0.6)	1.5 (0.3)	0.7 (0.2)	0.9 (0.4)
s6	39.0 (0.6)	109.8 (0.6)	37.5 (0.8)	38.3 (0.9)	1.0 (0.0)	32.2 (2.1)	9.4 (3.9)	39.9 (7.7)	0.8 (0.1)	4.0 (1.2)	3.5 (1.2)	2.1 (0.4)	1.6 (0.6)
s7	40.3 (0.6)	109.0 (2.4)	38.6 (0.5)	41.3 (2.8)	1.1 (0.1)	32.9 (1.5)	3.5 (3.5)	34.3 (6.4)	0.7 (0.1)	1.9 (0.1)	2.2 (0.5)	1.2 (0.7)	0.9 (0.2)

bioRxiv preprint doi: https://doi.org/10.1101/843425; this version posted November 15, 2019. The copyright holder for this preprint (which was not certified by peer review) is the author/funder. All rights reserved. No reuse allowed without permission.

s8	37.7 (0.2)	103.1 (0.3)	37.1 (0.2)	47.9 (0.4)	1.3 (0.0)	35.4 (1.1)	3.0 (3.7)	22.4 (14.9)	0.6 (0.0)	2.7 (0.6)	2.9 (0.8)	1.3 (0.4)	1.2 (0.3)
s9	41.3 (0.4)	106.6 (1.4)	40.0 (0.4)	44.6 (1.7)	1.1 (0.0)	33.9 (4.7)	6.8 (4.0)	35.9 (21.3)	0.7 (0.4)	1.9 (0.6)	2.1 (0.7)	1.0 (0.4)	0.9 (0.2)
s10	36.6 (0.2)	117.6 (0.9)	34.3 (0.2)	35.9 (0.9)	1.0 (0.0)	31.5 (1.2)	8.3 (0.9)	50.9 (4.1)	1.0 (0.1)	4.3 (1.6)	2.5 (0.4)	2.0 (0.8)	1.2 (0.2)
s11	34.2 (0.2)	114.7 (0.7)	33.1 (0.2)	35.7 (0.9)	1.1 (0.0)	36.4 (1.7)	0.0 (0.6)	4.5 (5.5)	0.2 (0.1)	2.0 (0.4)	1.6 (0.1)	1.2 (0.4)	0.9 (0.4)
s12	37.6 (0.4)	113.6 (1.5)	36.0 (0.4)	40.0 (1.7)	1.1 (0.0)	32.0 (1.1)	1.6 (1.6)	26.0 (4.9)	0.8 (0.1)	2.6 (0.4)	2.7 (0.6)	1.6 (0.4)	1.3 (0.4)
s13	36.3 (0.6)	109.1 (3.7)	34.1 (0.5)	44.4 (4.5)	1.3 (0.1)	31.8 (4.1)	3.7 (6.3)	15.8 (16.0)	0.4 (0.2)	1.9 (0.2)	2.0 (0.3)	1.0 (0.1)	1.0 (0.1)
s14	36.1 (0.9)	114.6 (0.9)	31.7 (0.6)	38.1 (0.8)	1.2 (0.0)	35.7 (0.8)	3.6 (1.6)	17.2 (4.4)	0.4 (0.1)	2.0 (0.9)	1.5 (0.3)	0.9 (0.1)	0.8 (0.2)
s15	35.8 (0.5)	115.9 (0.9)	32.8 (0.9)	37.7 (1.3)	1.2 (0.0)	34.1 (0.9)	7.9 (5.3)	30.7 (8.4)	0.6 (0.1)	1.4 (0.2)	4.3 (4.1)	0.9 (0.1)	1.6 (0.9)
s16	34.8 (0.5)	119.9 (1.0)	31.4 (0.5)	23.9 (1.2)	0.8 (0.0)	27.7 (6.5)	1.6 (2.1)	11.8 (4.0)	0.3 (0.1)	1.3 (0.6)	1.3 (0.4)	0.7 (0.4)	0.6 (0.2)

Baseline mean values (SD) of $P_{ET}CO_2$, $P_{ET}O_2$, ΔPCO_2, ΔPO_2 and bER for all subjects (n=16) who were under breath hold challenge in the MRI sessions (*left*). The averaged changes (SD) breath hold duration, ΔPCO_2, ΔPO_2, bER, ΔBOLD measured in LGM, RGM, LWM and RWM from the onset to the end of the breath hold epochs in the MRI sessions (*right*).

bioRxiv preprint doi: https://doi.org/10.1101/843425; this version posted November 15, 2019. The copyright holder for this preprint (which was not certified by peer review) is the author/funder. All rights reserved. No reuse allowed without permission.

bioRxiv preprint doi: https://doi.org/10.1101/843425; this version posted November 15, 2019. The copyright holder for this preprint (which was not certified by peer review) is the author/funder. All rights reserved. No reuse allowed without permission.

Correlation among RGE metrics

The correlations among the RGE metrics (bER, ΔPCO_2, ΔPO_2, $P_{ET}CO_2$, $P_{ET}O_2$, and ToB) in TCD and MRI sessions are shown in S1 Fig. Very strong correlation was found between bER and ΔPO_2 consistently in all subjects (Pearson's r, 0.70-0.98, $p<0.001$), while the correlation between bER and ΔPCO_2 varied from weak to moderate (Pearson's r, 0.07-0.75) (S1 Table). Moderate to strong correlation was observed between ΔPO_2 and ΔPCO_2 (Pearson's r, 0.44-0.88), and between $P_{ET}O_2$ and $P_{ET}CO_2$ (Pearson's r, 0.46-0.91). Such correlations suggest that ΔPO_2 and ΔPCO_2 (or $P_{ET}O_2$ and $P_{ET}CO_2$) are not necessarily redundant. Similar observation of non-redundancy between $P_{ET}O_2$ and $P_{ET}CO_2$ (correlation coefficients, 0.25-0.93) during spontaneous breathing was also reported by Lenfant et al. [52]. The different ranges of correlation strength observed between ΔPO_2 and ΔPCO_2 in the TCD and MRI sessions may be due to the interaction of the subjects with the environment. Subjects were sitting in an open and quiet environment in the TCD sessions while they were in supine position in a noisy MRI scanner bore. Many previous studies reported that a change from supine posture to sitting upright was associated with a redistribution of both blood flow and ventilation in the lungs, which affected the arterial PO_2 [53-56]. While it is interesting to observe a difference in the interaction between

bioRxiv preprint doi: https://doi.org/10.1101/843425; this version posted November 15, 2019. The copyright holder for this preprint (which was not certified by peer review) is the author/funder. All rights reserved. No reuse allowed without permission.

subjects and environment, the details of such mechanisms are outside the scope of our current study.

Correlation between cerebral hemodynamic responses and respiratory gas exchange metrics

Fig 2A shows the time series of ΔCBFv in left MCA and physiological changes including bER, ΔPO_2, ΔPCO_2, ToB, $P_{ET}O_2$ and $P_{ET}CO_2$ in a representative subject under breath hold challenge, while Fig 2B shows the time series of ΔBOLD in left gray matter, and the corresponding changes in RGE metrics in the same representative subject. The time series of bER followed the ΔCBFv and ΔBOLD closely in the subject. By visual inspection of the time series of ΔCBFv and ΔBOLD, the interpolated values of $P_{ET}CO_2$ and ΔPCO_2 during breath hold periods did not necessarily follow the changes of ΔCBFv and ΔBOLD.

Fig 2. Time series of cerebral hemodynamic responses and RGE metrics in a representative subject under breath hold challenge. (A) Time series of ΔCBFv in left MCA and physiological changes including breath-by-breath bER, ΔPO_2, ΔPCO_2, ToB,

bioRxiv preprint doi: https://doi.org/10.1101/843425; this version posted November 15, 2019. The copyright holder for this preprint (which was not certified by peer review) is the author/funder. All rights reserved. No reuse allowed without permission.

$P_{ET}O_2$ and $P_{ET}CO_2$ in a representative subject under breath hold challenge in TCD session. (B) Time series of ΔBOLD in left gray matter (LGM) and the corresponding physiological changes in the same representative subject under breath hold challenge in MRI session. Shaded areas represent breath hold periods. The time series of bER followed closely to the ΔCBFv and ΔBOLD changes, while ΔPO_2 did not follow ΔCBFv and ΔBOLD changes some time during the challenges as indicated by two-headed arrows in red. Thin green lines represent partial pressure of O_2, while the thin blue lines represent partial pressure of CO_2. Thick green lines and thick blue lines represent $P_{ET}O_2$ and $P_{ET}CO_2$ respectively.

Among the four RGE metrics of bER, ΔPO_2, ΔPCO_2 and ToB, bER is the only parameter that consistently showed strong correlation with the ΔCBFv measured in left and right MCAs (Pearson's r, 0.40-0.89, $p<0.001$) (Fig 3A). The bER also correlated with ΔBOLD extracted from gray (LGM and RGM) and white matter (LWM and RWM) under breath hold challenge (Pearson's r, 0.21-0.83, $p<0.05$), except one subject in the left brain (Pearson's r, -0.011-0.18, $p>0.05$) (Fig 3A). The results of correlation analyses between cerebral hemodynamic responses and RGE metrics were summarized in S2 Table. Group comparisons of the correlation between cerebral hemodynamic responses (ΔCBFv and ΔBOLD) and RGE metrics (bER, ΔPO_2, ΔPCO_2 and ToB) also showed that the correlation

bioRxiv preprint doi: https://doi.org/10.1101/843425; this version posted November 15, 2019. The copyright holder for this preprint (which was not certified by peer review) is the author/funder. All rights reserved. No reuse allowed without permission.

between cerebral hemodynamic responses and bER was significantly stronger than those between cerebral hemodynamic responses and the RGE metrics other than bER (S2 Table). Although ToB was not as good as bER in correlating with ΔCBFv or ΔBOLD, it was better than ΔPCO_2 to serve as an indicator of the breath hold periods.

Fig 3. Correlation and coherence between cerebral hemodynamic responses and RGE metrics in all subjects under breath hold challenge. (A) Strength of correlation between cerebral hemodynamic responses and respiratory metrics including bER, ΔPO_2, ΔPCO_2 and ToB. Top panel shows the correlation with ΔCBFv in LMCA and RMCA (n=12), the middle panel shows the correlation with ΔBOLD in LGM and RGM (n=16), and the bottom panel shows the correlation with ΔBOLD in LWM and RWM (n=16). Each grey circle represents the Pearson's correlation coefficient from the correlation analysis of the parameter pairs shown on x-axis for each subject. The thick horizontal black line, the box and the vertical rod represent the mean, standard deviation and 95% confidence interval of the group data respectively. The cerebral hemodynamic responses correlate with the respiratory metrics consistently in a descending order of bER, ΔPO_2, ToB and ΔPCO_2. (B) Distribution of time-averaged coherence at the phase lag $0\pm\pi/2$ between time series of respiratory metrics (bER, ΔPO_2, ΔPCO_2 and ToB) and cerebral hemodynamic responses.

bioRxiv preprint doi: https://doi.org/10.1101/843425; this version posted November 15, 2019. The copyright holder for this preprint (which was not certified by peer review) is the author/funder. All rights reserved. No reuse allowed without permission.

Top panel shows the coherence with ΔCBFv in LMCA and RMCA (n=12), the middle panel shows the coherence with ΔBOLD in LGM and RGM (n=16), and the bottom panel shows the coherence with ΔBOLD in LWM and RWM (n=16). The mean time-averaged coherence in the frequency bandwidths from 0.008 to 0.25Hz were plotted (thick color lines). Color shaded areas represent standard error of the mean. The mean time-averaged coherence between bER and cerebral hemodynamic responses reached 0.6 or above at the frequency range from 0.008Hz (1/128 seconds) to 0.03Hz (1/32 seconds), while the mean time-averaged coherence between ΔPCO_2 and cerebral hemodynamic responses stayed below 0.4. Comparing with ΔPCO_2, the mean time-averaged coherence of ΔPO_2 with cerebral hemodynamic responses reached 0.5 or above in the frequency range of 0.008-0.03Hz, which was better than that of ΔPCO_2.

Dynamic analysis of coherence between cerebral hemodynamic responses and RGE metrics as function of time and frequency

The mean time-averaged coherence between time series of RGE metrics (bER, ΔPO_2, ΔPCO_2 and ToB) and cerebral hemodynamic responses (ΔCBFv and ΔBOLD) was found to be significantly stronger between 0.008Hz (1/128 seconds) and 0.03Hz (1/32

bioRxiv preprint doi: https://doi.org/10.1101/843425; this version posted November 15, 2019. The copyright holder for this preprint (which was not certified by peer review) is the author/funder. All rights reserved. No reuse allowed without permission.

seconds) at phase lag of $0\pm\pi/2$ (S3 Fig). We therefore focused on the distribution of time-averaged coherence between RGE metrics and cerebral hemodynamic responses at the phase lag of $0\pm\pi/2$ (Fig 3). Among the 4 RGE metrics, the mean time-averaged coherence between bER and cerebral hemodynamic responses at phase lag of $0\pm\pi/2$ was the strongest at the frequency bandwidths of 0.008-0.03 Hz while that between ΔPCO_2 and cerebral hemodynamic responses was the weakest at the same frequency bandwidths. The mean time-averaged coherence between bER, ΔPO_2, ToB and cerebral hemodynamic responses at phase lag of $0\pm\pi/2$ reached 0.6 or above. at the frequency bandwidths of 0.008-0.03 Hz. The correlation and dynamic coherence results suggest that CBFv and BOLD signals oscillated with bER at a broad frequency range of low frequencies when the subjects were performing breath hold task. The differences in the correlation and coherence findings between ΔPO_2 and ΔPCO_2 further suggest that changes of PO_2 and PCO_2 are not simply the inverse of each other.

Part 2:

Group comparison of CVR between breath hold and exogenous CO_2 challenges

bioRxiv preprint doi: https://doi.org/10.1101/843425; this version posted November 15, 2019. The copyright holder for this preprint (which was not certified by peer review) is the author/funder. All rights reserved. No reuse allowed without permission.

Fig 4 shows the regional CVR brain maps averaged across 16 subjects who performed breath hold task in MRI sessions. Under breath hold challenge, most of the brain regions showed significant increase in $CVR_{BH\text{-}bER}$ and $CVR_{BH\text{-}ToB}$ especially in thalamus, insula and putamen, while no significant changes of $CVR_{BH\text{-}PETCO2}$ were observed in the same subject group (Fig 4).

Fig 4. Group CVR maps ($CVR_{BH\text{-}PETCO2}$, $CVR_{BH\text{-}ToB}$ and $CVR_{BH\text{-}bER}$) generated by regressing ΔBOLD separately on $P_{ET}CO_2$, ToB and bER under breath hold challenges (n=16). All the CVR maps had been corrected for $p_{fdr}<0.05$. Maps of $CVR_{BH\text{-}ToB}$ and $CVR_{BH\text{-}bER}$ were comparable, while $P_{ET}CO_2$ was not able to characterize the regional ΔBOLD.

In the comparison of CVR brain maps under breath hold and exogenous CO_2 challenge, a subset of 10 subjects who participated in both challenges were included. Under exogenous CO_2 challenge, most of the brain regions showed increased $CVR_{CO2\text{-}PETCO2}$ in the subject group especially thalamus, insula and putamen (Fig 5A), and the $vCVR_{CO2\text{-}PETCO2}$ which had significant $CVR_{CO2\text{-}PETCO2}$ changes exceeded 80% in most of the brain regions (Fig 5B). For the same group of subjects under breath hold challenge,

bioRxiv preprint doi: https://doi.org/10.1101/843425; this version posted November 15, 2019. The copyright holder for this preprint (which was not certified by peer review) is the author/funder. All rights reserved. No reuse allowed without permission.

increased $CVR_{BH\text{-}bER}$ and $CVR_{BH\text{-}ToB}$ were found in most of the brain regions, while no significant changes of $CVR_{BH\text{-}PETCO2}$ were shown in most of the brain regions (Fig 5A). CVR brain maps under breath hold challenge shown in Fig 5A (n=10) were consistent with those shown in Fig 4 (n=16). Comparing with the $vCVR_{BH\text{-}ToB}$ and $vCVR_{BH\text{-}PETCO2}$, $vCVR_{BH\text{-}bER}$ showed the largest percentage of voxels with significant CVR changes in different brain regions, implying a significantly high precision of bER predicting regional ΔBOLD in breath hold challenge (Fig 5B). The paired comparison between $vCVR_{CO2\text{-}PETCO2}$ and $vCVR_{BH\text{-}bER}$, as well as that between $vCVR_{CO2\text{-}PETCO2}$ and $vCVR_{BH\text{-}ToB}$, did not show significant difference in most of the brain regions, while significant differences were found in most of the brain regions between $vCVR_{CO2\text{-}PETCO2}$ and $vCVR_{BH\text{-}PETCO2}$ (Fig 5C). Such findings suggest that bER in breath hold challenge is more appropriate to be used as vasoactive stimulus than $P_{ET}CO_2$ in assessing regional CVR under breath hold challenge.

Fig 5. Comparison of group CVR maps under exogenous CO_2 challenge with those under breath hold challenge. (A) Group CVR showing significant CVR changes under exogenous CO_2 and breath hold challenges (n=10). Group map of $CVR_{BH\text{-}PETCO2}$ indicated that ΔBOLD in most of the brain regions did not associate with changes of $P_{ET}CO_2$ under breath hold challenge. (B) Group vCVR maps showing percentage of voxels with

bioRxiv preprint doi: https://doi.org/10.1101/843425; this version posted November 15, 2019. The copyright holder for this preprint (which was not certified by peer review) is the author/funder. All rights reserved. No reuse allowed without permission.

significant CVR changes under exogenous CO2 and breath hold challenges for the same group of subjects (n=10). The percentage of voxels with significant CVR changes under breath hold challenge were found in an increasing order of $vCVR_{BH\text{-}PETCO2}$, $vCVR_{BH\text{-}ToB}$ and $vCVR_{BH\text{-}bER}$. $CVR_{BH\text{-}bER}$ and $vCVR_{BH\text{-}bER}$ showed large resemblance with $CVR_{CO2\text{-}PETCO2}$ and $vCVR_{CO2\text{-}PETCO2}$ respectively. (C) Paired comparisons of vCVR maps showed that $vCVR_{CO2\text{-}PETCO2}$ maps under exogenous CO_2 challenge were not significantly different from $vCVR_{BH\text{-}bER}$ maps under breath hold challenge. Group map of $vCVR_{BH\text{-}PETCO2}$ showed that ΔBOLD in only small number of voxels within the brain regions associated with the $P_{ET}CO_2$ changes under breath hold challenge, resulting in significant differences found in multiple brain regions in the paired comparison between $vCVR_{CO2\text{-}PETCO2}$ and $vCVR_{BH\text{-}PETCO2}$.

bioRxiv preprint doi: https://doi.org/10.1101/843425; this version posted November 15, 2019. The copyright holder for this preprint (which was not certified by peer review) is the author/funder. All rights reserved. No reuse allowed without permission.

Discussion

Our findings show a strong positive correlation between the cerebral hemodynamic responses and our new breath-by-breath O_2-CO_2 exchange ratio, in short bER, under brief breath hold challenge. We are the first to show that the dynamic changes in bER robustly characterized CBFv and BOLD responses much better than changes in $P_{ET}CO_2$ or ToB under breath hold challenge in the very low frequency range of 0.008-0.03Hz. The difference between bER and ΔPCO_2 in coherence with cerebral hemodynamic responses within the frequency range of 0.008-0.03 Hz cannot be attributed to the long periods of the breath hold protocol alone since the influence of the periods of the breath hold protocol should contribute equally to all RGE metrics. During breath holding, we presented the combined effect of both hypoxia and hypercapnia on the cerebral hemodynamic responses measured using TCD and BOLD-fMRI. Given that the concurrent changes of $P_{ET}O_2$ and $P_{ET}CO_2$ are in opposite direction and the magnitudes depend on the respiratory phase and volume, ΔPO_2 and ΔPCO_2 were in phase and selected here to more conveniently characterize the breath-by-breath changes during breath holding and spontaneous breathing epochs. In characterizing regional BOLD signal changes to brief breath hold challenge, bER which took into account the interaction of ΔPO_2 and ΔPCO_2 yielded much better results than what $P_{ET}CO_2$ and ToB could do as we showed that the brain regions outlined

bioRxiv preprint doi: https://doi.org/10.1101/843425; this version posted November 15, 2019. The copyright holder for this preprint (which was not certified by peer review) is the author/funder. All rights reserved. No reuse allowed without permission.

by bER during brief breath hold challenge were comparable with those outlined by the $P_{ET}CO_2$ during exogenous CO_2 challenge.

Mild hypoxia enhances sensitivity of CBF changes to CO_2

During breath holding periods, the CO_2 release are dependent on O_2 uptake in the closed circuit of systemic circulation created by holding one's breath. The interaction between ΔPO_2 and ΔPCO_2 during breath hold is mainly resulting from the systemic metabolic process and different from the effect of exogenous gas administration which is primarily indicated by an increase in ΔPCO_2. In the current study, ΔPO_2 could go from 11 to 51 mmHg and ΔPCO_2 could go from 2 to 10 mmHg at the end of 30 seconds of breath holding in the TCD and MRI sessions (Tables 2A and B). This relatively modest level of change in ΔPO_2 had been reported to be able to induce a progressive increase of CBF in the presence of mild hypercapnia [57, 58]. Our findings of ΔPO_2 vs. ΔPCO_2 support the synergistic effect of hypoxia and hypercapnia on CBF change under breath hold challenge which are in parallel with the increased chemoreceptor activities in the presence of both mild hypoxia and mild hypercapnia reported by several research teams on animal models [20, 25, 26, 59]. Sensitivity of peripheral chemoreceptor at carotid body to arterial PCO_2

bioRxiv preprint doi: https://doi.org/10.1101/843425; this version posted November 15, 2019. The copyright holder for this preprint (which was not certified by peer review) is the author/funder. All rights reserved. No reuse allowed without permission.

was found to increase when there was a decrease in the level of arterial PO_2 in these studies [20, 25, 26, 59]. The chemoreceptor activity in response to arterial PO_2 took place at all levels of PO_2 ranging from hypoxia to normoxia and then up to 190mmHg or even higher in the range of hyperoxia. The chemoreceptor response curve to PO_2 was similar to a hyperbola with chemoreceptor activity rising faster under hypoxia (below 95mmHg) than under normoxia or hyperoxia [59]. Modulation of peripheral chemoreceptor activities may be expected to lead to modulation of CBF while their physiological mechanisms remain to be clarified.

Wavelet transform coherence (WTC) analysis showed strong coherence between bER and cerebral hemodynamic responses (ΔCBFv and ΔBOLD) under breath hold challenge

We used wavelet transform coherence analysis to examine the temporal features and frequency characteristics of bER, ΔPO_2, ΔPCO_2 and ToB, and their coherence with CBFv and BOLD signal changes under breath hold challenge. Using WTC, we showed that the coherence between cerebral hemodynamic responses (both ΔCBFv and ΔBOLD) and change in bER was much stronger than that between cerebral hemodynamic responses and

bioRxiv preprint doi: https://doi.org/10.1101/843425; this version posted November 15, 2019. The copyright holder for this preprint (which was not certified by peer review) is the author/funder. All rights reserved. No reuse allowed without permission.

change in ΔPCO_2 in a wide frequency range of 0.008-0.03Hz (Fig 3). The meaning of the range of 0.008-0.03Hz is best appreciated by examining the WTC findings which showed that bER and ΔPCO_2 were very different in the frequency distribution of their coherence with cerebral hemodynamic responses. The special characteristics of the frequency range of 0.008-0.03Hz need to be considered in the context of each individual RGE metric (ΔPO_2, ΔPCO_2 and bER) separately.

Comparing with ΔPCO_2, the stronger coherence found between bER and cerebral hemodynamic responses in low frequency range of 0.008-0.03Hz may be associated with low frequency physiological processes in the brain that are grouped in B-wave frequency bandwidth. B-waves with a period of 0.5 to 2 minutes have been reported to be related to autoregulation of microvasculature and spontaneous rhythmic oscillations in intracranial pressure [60, 61]. Changes in systemic PO_2 and PCO_2 may trigger the underlying mechanisms which involve the interaction of central and peripheral respiratory chemoreceptors as well as autonomic system to regulate CBF. B-waves may be associated in such a process through the contractile properties of pericytes or vascular smooth muscle cells to alter vascular diameter and ensure the delivery of O_2 and other circulating metabolites [62-65]. As autoregulation of CBF and oxygen delivery are the outcomes in this part of vital homeostatic process [20], it is reasonable that the stronger coupling was

bioRxiv preprint doi: https://doi.org/10.1101/843425; this version posted November 15, 2019. The copyright holder for this preprint (which was not certified by peer review) is the author/funder. All rights reserved. No reuse allowed without permission.

found between bER and cerebral hemodynamic responses, and between ΔPO_2 and cerebral hemodynamic responses.

In summary, among the four RGE metrics of bER, ΔPO_2, ΔPCO_2 and ToB, the cerebral hemodynamic responses showed the strongest correlation and dynamic coherence with bER, followed by ΔPO_2, ToB, and ΔPCO_2. A wide range of correlations found between ΔPO_2 and ΔPCO_2 (and between $P_{ET}O_2$ and $P_{ET}CO_2$) in the subject group, as well as the differences in the correlation in the time domain and coherence findings in wavelet transform coherence analysis between ΔPO_2 and ΔPCO_2 indicate that PO_2 and PCO_2 are not simply inverse of each other. The strong correlation between bER and ΔPO_2 (S1 Fig) indicates that bER is predominantly affected by ΔPO_2. ToB yielded superior correlation result than ΔPCO_2 because ToB indirectly takes into account the duration for both hypoxemia and hypercapnia which both elevate cerebral hemodynamic responses without being affected by the depth of breathing. bER is the most accurate in characterizing cerebral hemodynamic responses under breath hold challenge because it directly takes into account the effect of both ΔPO_2 and ΔPCO_2.

bioRxiv preprint doi: https://doi.org/10.1101/843425; this version posted November 15, 2019. The copyright holder for this preprint (which was not certified by peer review) is the author/funder. All rights reserved. No reuse allowed without permission.

CVR map from breath hold challenge resembled that from exogenous CO_2 challenge

Our CVR findings showed that there was a large resemblance between regional $CVR_{BH\text{-}bER}$ and $CVR_{CO2\text{-}PETCO2}$, even though the underlying physiological mechanisms for the CBF increase are potentially different (Fig 5). From spontaneous breathing to breath holding periods, the bER, ΔPO_2 and ΔPCO_2 measured were due to endogenous changes of respiratory gases involved in the process of systemic metabolism. Previous studies reported that apnea-induced hypoxia and hypercapnia caused chemoreceptor-mediated central vasodilation and concurrent peripheral vasoconstriction to conserve oxygen delivery to the brain [15], leading to an increase in CBF and a decrease in peripheral oxygen saturation [29]. In our current study, cerebral hemodynamic responses were shown to be elevated accompanied by reduced oxygen saturation (data not shown) by concurrent hypoxia and hypercapnia. Holding breath is different from exogenous CO_2 administration where ΔPO_2 and ΔPCO_2 from normocapnic to hypercapnic epochs depended on the externally administered gas mixture and the increase in cerebral hemodynamic responses was mainly due to hypercapnia. One explanation for the large resemblance of the CVR maps between the breath hold and exogenous CO_2 challenges is that bER as an optimal regressor under breath hold challenge is able to characterize the increase in cerebral

bioRxiv preprint doi: https://doi.org/10.1101/843425; this version posted November 15, 2019. The copyright holder for this preprint (which was not certified by peer review) is the author/funder. All rights reserved. No reuse allowed without permission.

hemodynamic responses in most of the brain regions. Comparing the brain maps of $vCVR_{BH\text{-}bER}$ with those of $vCVR_{BH\text{-}ToB}$ and $vCVR_{BH\text{-}PETCO2}$, more voxels showed significant association between ΔBOLD and bER. For CVR maps, $CVR_{BH\text{-}ToB}$ resembled $CVR_{CO2\text{-}PETCO2}$ more than $CVR_{BH\text{-}PETCO2}$ did because ToB is a good time indicator of breath hold epochs as shown in Fig 2.

Breath hold challenge, as shown in our findings in Part 2, was able to offer significant regional CVR quantification, as long as the proper regressor was used. Since bER is a measure of the dynamic change of RGE which is related to ratio of the change of partial pressure in O_2 uptake to that in CO_2 production in the body, mapping CVR to breath hold may offer a novel probe to study the interaction between brain responses and some measures of systemic metabolism. Mild exogenous CO_2 challenge is expected to have little effect on cerebral [66] and presumably systemic metabolism. From a technical approach, breath-holding challenge for CVR assessment is much easier to set up in clinical settings than external CO_2 administration which requires an elaborate gas administration circuit [6]. The breath-holding challenge also allows patients to switch back to normal breathing whenever their physiological limit is reached [14]. In patients who have compromised vasculature with potential risk of acute intracranial hemorrhage, breath-holding may offer

bioRxiv preprint doi: https://doi.org/10.1101/843425; this version posted November 15, 2019. The copyright holder for this preprint (which was not certified by peer review) is the author/funder. All rights reserved. No reuse allowed without permission.

an option for CVR study if one has some yet-to-be proven concern over the more powerful physiological stress presented by rapid increase of externally administered CO_2.

Why was the ratio of ΔPO_2 to ΔPCO_2 used, and not the product?

The success of bER in better characterizing dynamic CBFv and BOLD signal changes under breath hold challenge is closely related to the fact that bER is a ratio which factors out at the same time effects of ventilatory volume fluctuations [67] common to both ΔPO_2 and ΔPCO_2. Given that both hypoxia and hypercapnia induce the increase in cerebral hemodynamic responses, one may wonder whether the product of ΔPO_2 and ΔPCO_2 would be better than bER for the evaluation of change in cerebral hemodynamic responses. Our answer is no. First, the product of ΔPO_2 and ΔPCO_2 would exacerbate the contribution of fluctuations from ventilatory volume. Secondly, unlike the ratio which has long been used to properly describe RGE since at least 1913 [68], the product does not have an established physiological meaning. Actually, another way to look at bER is that it describes the change of ΔPO_2 per unit change of ΔPCO_2, so the ratio provides a way to quantify how O_2 and CO_2 can work together to interact with cerebral hemodynamic responses.

bioRxiv preprint doi: https://doi.org/10.1101/843425; this version posted November 15, 2019. The copyright holder for this preprint (which was not certified by peer review) is the author/funder. All rights reserved. No reuse allowed without permission.

Conclusion

Independent of our current knowledge to completely clarify why bER offers the strongest association with cerebral hemodynamic responses to breath holding, we succeeded in showing that bER was superior to ΔPCO_2 or $P_{ET}CO_2$ to characterize cerebral hemodynamic responses under breath hold challenge for the CVR evaluation. RGE metrics of both ΔPO_2 and ΔPCO_2 should always be acquired for CVR evaluation instead of acquiring $P_{ET}CO_2$ data alone. In addition to offering alternative approach of CVR evaluation for patients who are not eligible for exogenous CO_2 challenge, the association between bER and cerebral hemodynamic responses also provides a novel insight in the study of brain-body interaction. Future studies would be required to clarify the underlying mechanisms for the relationship between dynamic bER and cerebral hemodynamic response to breath holding. Studies to quantify the relationship between changes in cerebral hemodynamic responses during breath holding and changes in bER in a large cohort of subjects and patients would be helpful to explore the effects on CVR by various disorders including respiratory or cerebral diseases with neurovascular deficits.

bioRxiv preprint doi: https://doi.org/10.1101/843425; this version posted November 15, 2019. The copyright holder for this preprint (which was not certified by peer review) is the author/funder. All rights reserved. No reuse allowed without permission.

Funding

This research was carried out in whole at the Athinoula A. Martinos Center for Biomedical Imaging at the Massachusetts General Hospital, using resources provided by the Center for Functional Neuroimaging Technologies, P41EB015896, a P41 Biotechnology Resource Grant supported by the National Institute of Biomedical Imaging and Bioengineering (NIBIB), National Institutes of Health, as well as the Shared Instrumentation Grant S10RR023043. This work was also supported, in part, by NIH-K23MH086619.

bioRxiv preprint doi: https://doi.org/10.1101/843425; this version posted November 15, 2019. The copyright holder for this preprint (which was not certified by peer review) is the author/funder. All rights reserved. No reuse allowed without permission.

References

1. Kastrup A, Li TQ, Glover GH, Moseley ME. Cerebral blood flow-related signal changes during breath-holding. AJNR Am J Neuroradiol. 1999;20(7):1233-8.

2. Markus HS, Harrison MJ. Estimation of cerebrovascular reactivity using transcranial Doppler, including the use of breath-holding as the vasodilatory stimulus. Stroke. 1992;23(5):668-73.

3. Ratnatunga C, Adiseshiah M. Increase in middle cerebral artery velocity on breath holding: a simplified test of cerebral perfusion reserve. European journal of vascular surgery. 1990;4(5):519-23.

4. Vernieri F, Pasqualetti P, Passarelli F, Rossini PM, Silvestrini M. Outcome of carotid artery occlusion is predicted by cerebrovascular reactivity. Stroke. 1999;30(3):593-8.

5. Silvestrini M, Vernieri F, Troisi E, Passarelli F, Matteis M, Pasqualetti P, et al. Cerebrovascular reactivity in carotid artery occlusion: possible implications for surgical

bioRxiv preprint doi: https://doi.org/10.1101/843425; this version posted November 15, 2019. The copyright holder for this preprint (which was not certified by peer review) is the author/funder. All rights reserved. No reuse allowed without permission.

management of selected groups of patients. Acta neurologica Scandinavica. 1999;99(3):187-91.

6. Pillai JJ, Mikulis DJ. Cerebrovascular reactivity mapping: an evolving standard for clinical functional imaging. AJNR American journal of neuroradiology. 2015;36(1):7-13.

7. Liu HL, Huang J, Wu CT, Hsu YY. Detectability of blood oxygenation level-dependent signal changes during short breath hold duration. Magn Reson Imaging. 2002;20(9):643-8.

8. Schmithorst VJ, Hernandez-Garcia L, Vannest J, Rajagopal A, Lee G, Holland SK. Optimized simultaneous ASL and BOLD functional imaging of the whole brain. J Magn Reson Imaging. 2014;39(5):1104-17.

9. Cooper HE, Parkes MJ, Clutton-Brock TH. CO2-dependent components of sinus arrhythmia from the start of breath holding in humans. Am J Physiol Heart Circ Physiol. 2003;285(2):H841-8.

10. Bright MG, Murphy K. Reliable quantification of BOLD fMRI cerebrovascular reactivity despite poor breath-hold performance. NeuroImage. 2013;83:559-68.

bioRxiv preprint doi: https://doi.org/10.1101/843425; this version posted November 15, 2019. The copyright holder for this preprint (which was not certified by peer review) is the author/funder. All rights reserved. No reuse allowed without permission.

11. Murphy K, Harris AD, Wise RG. Robustly measuring vascular reactivity differences with breath-hold: normalising stimulus-evoked and resting state BOLD fMRI data. NeuroImage. 2011;54(1):369-79.

12. Tancredi FB, Hoge RD. Comparison of cerebral vascular reactivity measures obtained using breath-holding and CO2 inhalation. Journal of Cerebral Blood Flow and Metabolism. 2013;33(7):1066-74.

13. Bain AR, Ainslie PN, Barak OF, Hoiland RL, Drvis I, Mijacika T, et al. Hypercapnia is essential to reduce the cerebral oxidative metabolism during extreme apnea in humans. J Cereb Blood Flow Metab. 2017;37(9):3231-42.

14. Parkes MJ. Breath-holding and its breakpoint. Exp Physiol. 2006;91(1):1-15.

15. Gooden BA. Mechanism of the human diving response. Integr Physiol Behav Sci. 1994;29(1):6-16.

16. Lassen NA. Cerebral blood flow and oxygen consumption in man. Physiol Rev. 1959;39(2):183-238.

bioRxiv preprint doi: https://doi.org/10.1101/843425; this version posted November 15, 2019. The copyright holder for this preprint (which was not certified by peer review) is the author/funder. All rights reserved. No reuse allowed without permission.

17. Shimojyo S, Scheinberg P, Kogure K, Reinmuth OM. The effects of graded hypoxia upon transient cerebral blood flow and oxygen consumption. Neurology. 1968;18(2):127-33.

18. Hoiland RL, Bain AR, Rieger MG, Bailey DM, Ainslie PN. Hypoxemia, oxygen content, and the regulation of cerebral blood flow. Am J Physiol Regul Integr Comp Physiol. 2016;310(5):R398-413.

19. Van den Aardweg JG, Karemaker JM. Influence of chemoreflexes on respiratory variability in healthy subjects. American journal of respiratory and critical care medicine. 2002;165(8):1041-7.

20. Kumar P, Prabhakar NR. Peripheral chemoreceptors: function and plasticity of the carotid body. Compr Physiol. 2012;2(1):141-219.

21. Guyenet PG, Stornetta RL, Bayliss DA. Central respiratory chemoreception. J Comp Neurol. 2010;518(19):3883-906.

22. Nattie E, Li A. Central chemoreceptors: locations and functions. Compr Physiol. 2012;2(1):221-54.

bioRxiv preprint doi: https://doi.org/10.1101/843425; this version posted November 15, 2019. The copyright holder for this preprint (which was not certified by peer review) is the author/funder. All rights reserved. No reuse allowed without permission.

23. Daristotle L, Berssenbrugge AD, Bisgard GE. Hypoxic-hypercapnic ventilatory interaction at the carotid body of awake goats. Respir Physiol. 1987;70(1):63-72.

24. Lahiri S, DeLaney RG. Stimulus interaction in the responses of carotid body chemoreceptor single afferent fibers. Respir Physiol. 1975;24(3):249-66.

25. Biscoe TJ, Purves MJ, Sampson SR. The frequency of nerve impulses in single carotid body chemoreceptor afferent fibres recorded in vivo with intact circulation. J Physiol. 1970;208(1):121-31.

26. Lahiri S, Mokashi A, Delaney RG, Fishman AP. Arterial PO2 and PCO2 stimulus threshold for carotid chemoreceptors and breathing. Respir Physiol. 1978;34(3):359-75.

27. Honda Y, Natsui T, Hasumura N, Nakamura K. Threshold Pco2 for Respiratory System in Acute Hypoxia of Dogs. J Appl Physiol. 1963;18:1053-6.

28. von Euler U, Liljestrand G, Zotterman Y. The excitation mechanism of the chemoreceptors of the carotid body. Scand Arch Physiol. 1939;83:132-52.

29. Rodgers ZB, Jain V, Englund EK, Langham MC, Wehrli FW. High temporal resolution MRI quantification of global cerebral metabolic rate of oxygen consumption in response to apneic challenge. J Cereb Blood Flow Metab. 2013;33(10):1514-22.

bioRxiv preprint doi: https://doi.org/10.1101/843425; this version posted November 15, 2019. The copyright holder for this preprint (which was not certified by peer review) is the author/funder. All rights reserved. No reuse allowed without permission.

30. Shapiro W, Wasserman AJ, Baker JP, Patterson JL, Jr. Cerebrovascular response to acute hypocapnic and eucapnic hypoxia in normal man. The Journal of clinical investigation. 1970;49(12):2362-8.

31. Mardimae A, Balaban DY, Machina MA, Battisti-Charbonney A, Han JS, Katznelson R, et al. The interaction of carbon dioxide and hypoxia in the control of cerebral blood flow. Pflugers Archiv : European journal of physiology. 2012;464(4):345-51.

32. Fenn WO, Rahn H, Otis AB. A theoretical study of the composition of the alveolar air at altitude. Am J Physiol. 1946;146:637-53.

33. Weir JB. New methods for calculating metabolic rate with special reference to protein metabolism. The Journal of physiology. 1949;109(1-2):1-9.

34. Nishi Y, editor. Measurement of thermal balance in man. New York. NY.: Elsevier; 1981.

35. Bain AR, Lesperance NC, Jay O. Body heat storage during physical activity is lower with hot fluid ingestion under conditions that permit full evaporation. Acta physiologica. 2012;206(2):98-108.

bioRxiv preprint doi: https://doi.org/10.1101/843425; this version posted November 15, 2019. The copyright holder for this preprint (which was not certified by peer review) is the author/funder. All rights reserved. No reuse allowed without permission.

36. Chobanian AV, Bakris GL, Black HR, Cushman WC, Green LA, Izzo JL, Jr., et al. The Seventh Report of the Joint National Committee on Prevention, Detection, Evaluation, and Treatment of High Blood Pressure: the JNC 7 report. JAMA. 2003;289(19):2560-72.

37. West JB. Pulmonary Pathophysiology. Baltimore: Williams & Wilkins; 1992.

38. Banzett RB, Garcia RT, Moosavi SH. Simple contrivance "clamps" end-tidal PCO(2) and PO(2) despite rapid changes in ventilation. J Appl Physiol. 2000;88(5):1597-600.

39. McKay LC, Evans KC, Frackowiak RS, Corfield DR. Neural correlates of voluntary breathing in humans. J Appl Physiol. 2003;95(3):1170-8.

40. Aaslid R, Markwalder TM, Nornes H. Noninvasive transcranial Doppler ultrasound recording of flow velocity in basal cerebral arteries. J Neurosurg. 1982;57(6):769-74.

41. Ringelstein EB, Kahlscheuer B, Niggemeyer E, Otis SM. Transcranial Doppler sonography: anatomical landmarks and normal velocity values. Ultrasound Med Biol. 1990;16(8):745-61.

bioRxiv preprint doi: https://doi.org/10.1101/843425; this version posted November 15, 2019. The copyright holder for this preprint (which was not certified by peer review) is the author/funder. All rights reserved. No reuse allowed without permission.

42. Deppe M, Knecht S, Henningsen H, Ringelstein EB. AVERAGE: a Windows program for automated analysis of event related cerebral blood flow. J Neurosci Methods. 1997;75(2):147-54.

43. Cox RW. AFNI: software for analysis and visualization of functional magnetic resonance neuroimages. Comput Biomed Res. 1996;29(3):162-73.

44. Fischl B, Sereno MI, Dale AM. Cortical surface-based analysis. II: Inflation, flattening, and a surface-based coordinate system. Neuroimage. 1999;9(2):195-207.

45. Torrence C, Compo GP. A Practical Guide to Wavelet Analysis. Bulletin of the American Meteorological Society. 1998;79(1):61-78.

46. Grinsted A, Moore JC, Jevrejeva S. Application of the cross wavelet transform and wavelet coherence to geophysical time series. Nonlinear Processes in Geophysics. 2004;11(561-6).

47. Ng EKW, Chan JCL. Geophysical applications of partial wavelet coherence and multiple wavelet coherence. Journal of Atmospheric and Oceanic Technology. 2012;29:1845-53.

bioRxiv preprint doi: https://doi.org/10.1101/843425; this version posted November 15, 2019. The copyright holder for this preprint (which was not certified by peer review) is the author/funder. All rights reserved. No reuse allowed without permission.

48. Zhang R, Zuckerman JH, Giller CA, Levine BD. Transfer function analysis of dynamic cerebral autoregulation in humans. Am J Physiol. 1998;274(1 Pt 2):H233-41.

49. Talairach J, Tournoux P. Co-Planar Stereotaxic Atlas of the Human Brain. New York: Thieme Medical; 1988.

50. Gold S, Christian B, Arndt S, Zeien G, Cizadlo T, Johnson DL, et al. Functional MRI statistical software packages: a comparative analysis. Hum Brain Mapp. 1998;6(2):73-84.

51. Ward LL. Simultaneous inference for fMRI data. Biophysics Research Institute, Medical College of Wisconsin; 1997.

52. Lenfant C. Time-dependent variations of pulmonary gas exchange in normal man at rest. J Appl Physiol. 1967;22(4):675-84.

53. Glaister DH. The effect of posture on the distribution of ventilation and blood flow in the normal lung. Clin Sci. 1967;33(2):391-8.

54. Amis TC, Jones HA, Hughes JM. Effect of posture on inter-regional distribution of pulmonary perfusion and VA/Q ratios in man. Respir Physiol. 1984;56(2):169-82.

bioRxiv preprint doi: https://doi.org/10.1101/843425; this version posted November 15, 2019. The copyright holder for this preprint (which was not certified by peer review) is the author/funder. All rights reserved. No reuse allowed without permission.

55. Petersson J, Rohdin M, Sanchez-Crespo A, Nyren S, Jacobsson H, Larsson SA, et al. Regional lung blood flow and ventilation in upright humans studied with quantitative SPECT. Respir Physiol Neurobiol. 2009;166(1):54-60.

56. Remolina C, Khan AU, Santiago TV, Edelman NH. Positional hypoxemia in unilateral lung disease. N Engl J Med. 1981;304(9):523-5.

57. Shapiro W, Wasserman AJ, Baker JP, Patterson JL, Jr. Cerebrovascular response to acute hypocapnic and eucapnic hypoxia in normal man. J Clin Invest. 1970;49(12):2362-8.

58. Mardimae A, Balaban DY, Machina MA, Battisti-Charbonney A, Han JS, Katznelson R, et al. The interaction of carbon dioxide and hypoxia in the control of cerebral blood flow. Pflugers Archiv. 2012;464(4):345-51.

59. Lahiri S, DeLaney RG. Relationship between carotid chemoreceptor activity and ventilation in the cat. Respir Physiol. 1975;24(3):267-86.

60. Lundberg N. Continuous recording and control of ventricular fluid pressure in neurosurgical practice. Acta psychiatrica Scandinavica Supplementum. 1960;36(149):1-193.

bioRxiv preprint doi: https://doi.org/10.1101/843425; this version posted November 15, 2019. The copyright holder for this preprint (which was not certified by peer review) is the author/funder. All rights reserved. No reuse allowed without permission.

61. Spiegelberg A, Preuß M, Kurtcuoglu V. B-waves revisited. Interdisciplinary Neurosurgery. 2016;6:13-7.

62. Zonta M, Angulo MC, Gobbo S, Rosengarten B, Hossmann KA, Pozzan T, et al. Neuron-to-astrocyte signaling is central to the dynamic control of brain microcirculation. Nature Neurosci. 2003;6(1):43-50.

63. Mulligan SJ, MacVicar BA. Calcium transients in astrocyte endfeet cause cerebrovascular constrictions. Nature. 2004;431(7005):195-9.

64. Takano T, Tian GF, Peng W, Lou N, Libionka W, Han X, et al. Astrocyte-mediated control of cerebral blood flow. Nature Neurosci. 2006;9(2):260-7.

65. Hill RA, Tong L, Yuan P, Murikinati S, Gupta S, Grutzendler J. Regional Blood Flow in the Normal and Ischemic Brain Is Controlled by Arteriolar Smooth Muscle Cell Contractility and Not by Capillary Pericytes. Neuron. 2015;87(1):95-110.

66. Kety SS, Schmidt CF. The effects of altered arterial tensions of carbon dioxide and oxygen on cerebral blood flow and cerebral oxygen consumption of normal young men. J Clin Invest. 1948;27(4):484-92.

bioRxiv preprint doi: https://doi.org/10.1101/843425; this version posted November 15, 2019. The copyright holder for this preprint (which was not certified by peer review) is the author/funder. All rights reserved. No reuse allowed without permission.

67. Ferretti G. Energetics of Muscular Exercise. Switzerland: Springer International Publishing; 2015.

68. Fitzgerald MP, Haldane JS. VIII. The changes in the breathing and the blood at various high altitudes. Philosophical Transactions of the Royal Society of London Series B, Containing Papers of a Biological Character. 1913;203(294-302):351-71.

bioRxiv preprint doi: https://doi.org/10.1101/843425; this version posted November 15, 2019. The copyright holder for this preprint (which was not certified by peer review) is the author/funder. All rights reserved. No reuse allowed without permission.

Supporting information

S1 Fig. Definition of end inspiration and end expiration on the time series of RGE metrics and the correlations among breath-by breath RGE matrices. (A) A segment of 80-second time series of ΔCBFv in left MCA and physiological changes including breath-by-breath bER, ΔPO_2, ΔPCO_2, $P_{ET}O_2$ and $P_{ET}CO_2$ measured by gas analyzers and respiration time series (Resp) measured by respiratory bellow in a representative subject under breath hold challenge in TCD session. Open circles represent end expiration while closed circles represent end inspiration in resting phase or onset of expiration at the end of breath hold epoch. Positive phases with deflection above zero on the respiration time series represent inspiration and negative phases with deflection below zero represent expiration. The inspiratory and expiratory phases of each respiratory cycle on the time series of $P_{ET}O_2$ and $P_{ET}CO_2$ are verified by those on respiration time series. The timing for open (end expiration) and closed (end inspiration) circles in green is the same as those in red and blue. (B) Correlations among breath-by breath respiratory matrices (bER, ΔPO_2, ΔPCO_2, ToB, $P_{ET}O_2$ and $P_{ET}CO_2$) in all subjects who participated in TCD sessions (n=12), and (C) those who participated in MRI sessions (n=16). Each gray circle represents the Pearson's correlation coefficient from the correlation analysis of the time series of parameter pair shown on x-axis for each subject. The thick middle horizontal line, the box and the vertical

bioRxiv preprint doi: https://doi.org/10.1101/843425; this version posted November 15, 2019. The copyright holder for this preprint (which was not certified by peer review) is the author/funder. All rights reserved. No reuse allowed without permission.

rod represent the mean, standard deviation and 95% confidence interval of the group data respectively. The time series of bER had stronger correlation with that of ΔPO_2 than ΔPCO_2, although both ΔPO_2 and ΔPCO_2 contributed to changes of bER. The correlation coefficients from ΔPO_2 vs ΔPCO_2 varied from 0.6 to 0.9 in TCD sessions and from 0.4 to 0.9 in MRI sessions, suggesting that ΔPO_2 and ΔPCO_2 are not necessarily redundant. The difference in the ranges of correlation strength found between TCD and MRI sessions may be due to the difference in posture of the subjects, where the subjects were in erect seated position in TCD sessions and they were in supine position in MRI sessions.

S2 Fig. Wavelet transform coherence analysis between bER and ΔCBFv in a representative subject. (A) Time series of bER and ΔCBFv measured in right MCA in a representative subject under breath hold challenge. (B) The squared wavelet coherence between these two time series. Squared wavelet coherence is plotted with x-axis as time and y-axis as scale which has been converted to its equivalent Fourier period. The magnitude of wavelet transform coherence ranges between 0 and 1, where warmer color represents stronger coherence and cooler color represents weaker coherence. Areas inside the 'cone of influence', which are locations in the time-frequency plane where edge effects give rise to lower confidence in the computed values, are shown in faded color outside of

bioRxiv preprint doi: https://doi.org/10.1101/843425; this version posted November 15, 2019. The copyright holder for this preprint (which was not certified by peer review) is the author/funder. All rights reserved. No reuse allowed without permission.

the conical contour. The statistical significance level of the wavelet coherence is estimated using Monte Carlo methods and the 5% significance level against red noise is shown as thick contour. The phase angle between the two time series at particular samples of the time-frequency plane is indicated by an arrow (rightward pointing arrows indicate that the time series are in phase or positively correlation, leftward pointing arrows indicate anticorrelation and the downward pointing arrows indicate phase angles of $\pi/2$). There are four different ranges of phase lags: $0+\pi/2$, $0-\pi/2$, $\pi-\pi/2$, and $\pi+\pi/2$. (C) Time-averaged coherences at four different phase lags of $0+\pi/2$, $0-\pi/2$, $\pi-\pi/2$, and $\pi+\pi/2$. At each phase lag range, time-averaged coherence was defined as the total significant coherence at each scale where the wavelet coherence magnitude exceeded 95% significance level, normalized by the maximum possible coherence outside the cone of influence, i.e. inside the conical contour, at that particular scale and phase lag range.

S3 Fig. Coherence between time series of RGE metrics and cerebral hemodynamic response at four different phase lags ($0+\pi/2$, $0-\pi/2$, $\pi-\pi/2$, and $\pi+\pi/2$). The mean time-averaged coherence between time series of respiratory metrics and cerebral hemodynamic responses (ΔCBFv in LMCA and RMCA, and ΔBOLD in LGM, RGM, LWM and RWM) at four different phase lags ($0+\pi/2$, $0-\pi/2$, $\pi-\pi/2$, and $\pi+\pi/2$) for the subjects included in the

bioRxiv preprint doi: https://doi.org/10.1101/843425; this version posted November 15, 2019. The copyright holder for this preprint (which was not certified by peer review) is the author/funder. All rights reserved. No reuse allowed without permission.

TCD sessions (n=12) and in the MRI sessions (n=16). Color shaded areas represent SEM. Comparing with ΔPO_2, ΔPCO_2 and ToB, the total time-averaged coherence between bER and cerebral hemodynamic responses was found to be significantly stronger between 0.008Hz (1/128 seconds) and 0.03Hz (1/32 seconds). The strong mean time-averaged coherence between respiratory metrics and cerebral hemodynamic responses were found at phase lag of $0+\pi/2$.

S1 Table. Correlation among RGE metrics. Strength of correlation indicated by Pearson's correlation coefficients among respiratory metrics including bER, ΔPO_2, ΔPCO_2, ToB, $P_{ET}O_2$ and $P_{ET}CO_2$ in all subjects who participated in TCD sessions (n=12), and those who participated in MRI sessions (n=16). The time series of bER had stronger correlation with that of ΔPO_2 than ΔPCO_2, although both ΔPO_2 and ΔPCO_2 contributed to changes of bER. The correlation coefficients from ΔPO_2 vs ΔPCO_2 varied from 0.6 to 0.9 in TCD sessions and from 0.4 to 0.9 in MRI sessions, suggesting that ΔPO_2 than ΔPCO_2 are not necessarily redundant.

S2 Table A. Correlation between RGE metrics and ΔCBFv in TCD sessions. Strength of correlation indicated by Pearson's correlation coefficients between ΔCBFv and RGE

bioRxiv preprint doi: https://doi.org/10.1101/843425; this version posted November 15, 2019. The copyright holder for this preprint (which was not certified by peer review) is the author/funder. All rights reserved. No reuse allowed without permission.

metrics including bER, ΔPO_2, ΔPCO_2 and ToB (n=12). Numbers in brackets next to Pearson's correlation coefficients indicate p values from individual correlation analyses. The bottom row shows the mean values of Fisher Z scores transformed from Pearson's correlation coefficients in groups. Numbers in brackets next to mean Fisher Z scores indicate p values in the paired comparisons. The correlation between ΔCBFv and bER was significantly larger than those of the correlation between ΔCBFv and the other respiratory metrics in the paired comparisons ($p<0.001$). bER is the only parameter that consistently showed significantly high correlation with the ΔCBFv measured in LMCA and RMCA.

S2 Table B. Correlation between RGE metrics and ΔBOLD in MRI sessions. Strength of correlation indicated by Pearson's correlation coefficients between ΔBOLD and RGE metrics including bER, ΔPO_2, ΔPCO_2 and ToB (n=16). Numbers in brackets next to Pearson's correlation coefficients indicate p values from individual correlation analyses. The bottom row shows the mean values of Fisher Z scores transformed from Pearson's correlation coefficients in groups. Numbers in brackets next to mean Fisher Z scores indicate p values in paired comparisons. The correlation between ΔBOLD and bER was significantly larger than those of the correlation between ΔBOLD and the other respiratory metrics in the paired comparisons ($p<0.001$). bER is the only parameter that consistently

bioRxiv preprint doi: https://doi.org/10.1101/843425; this version posted November 15, 2019. The copyright holder for this preprint (which was not certified by peer review) is the author/funder. All rights reserved. No reuse allowed without permission.

showed significantly high correlation with the ΔBOLD measured in LGM, RGM, LWM and RWM.

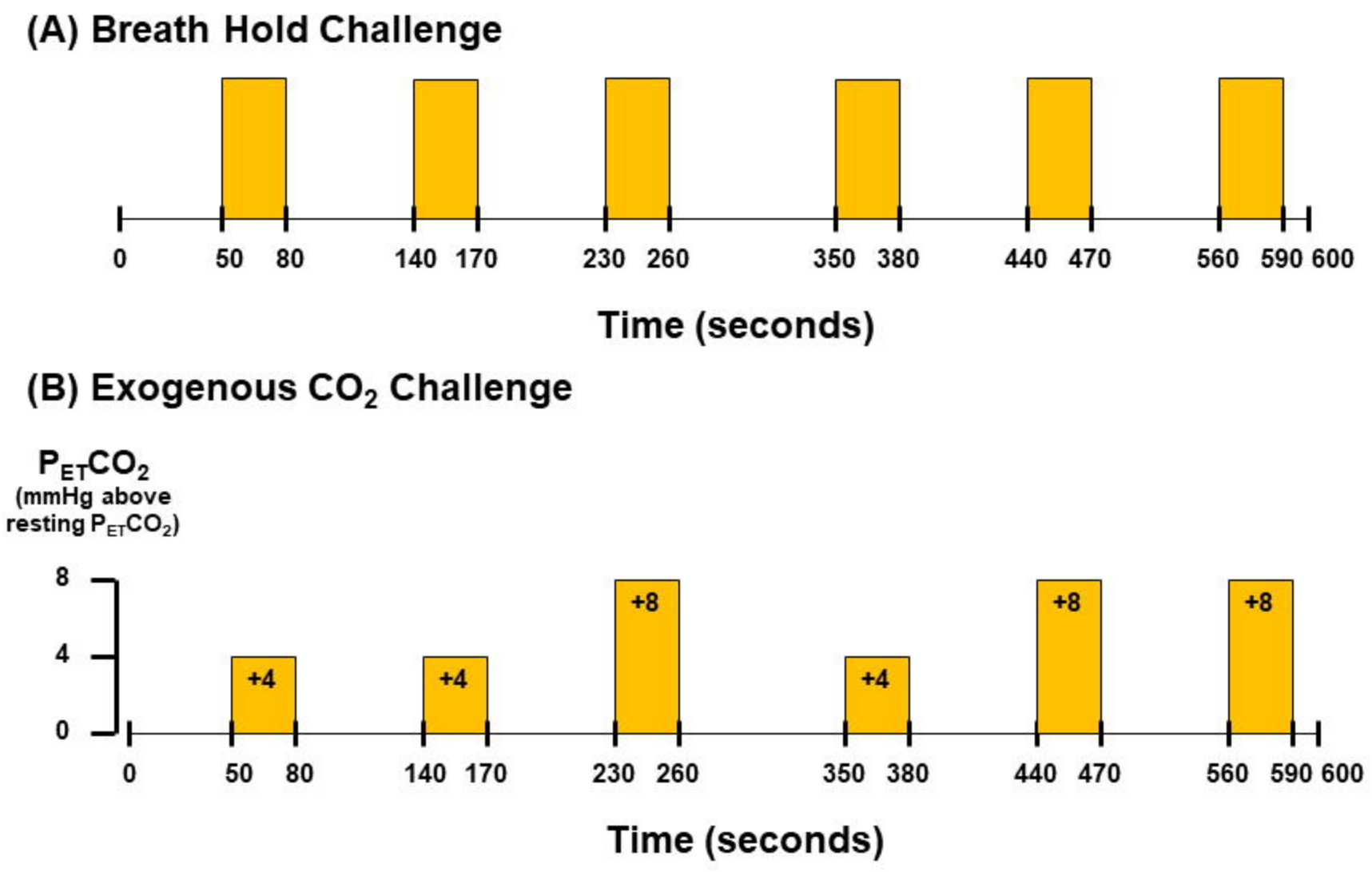
(A) Breath Hold Challenge
0
50
80
140
170
230
260
350
380
440
470
560
590
600
Time (seconds)
(B) Exogenous CO_2 Challenge
$P_{ET}CO_2$
(mmHg above
resting $P_{ET}CO_2$)
8
4
0
+4
+4
+8
+4
+8
+8
0
50
80
140
170
230
260
350
380
440
470
560
590
600
Time (seconds)

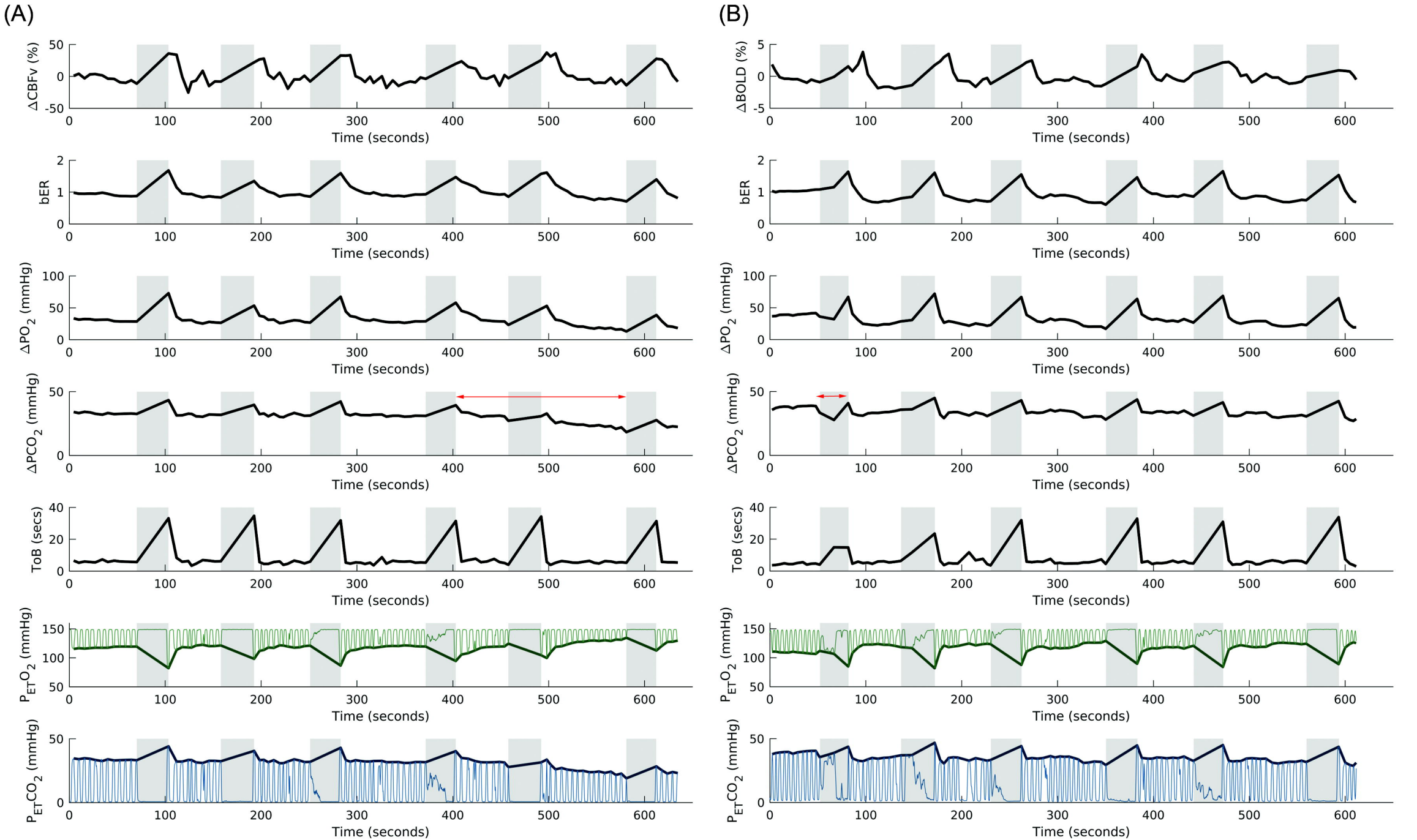
(A)
(B)
ΔCBFv (%)
ΔBOLD (%)
bER
ΔPO2 (mmHg)
ΔPCO2 (mmHg)
ToB (secs)
PETO2 (mmHg)
PETCO2 (mmHg)
Time (seconds)

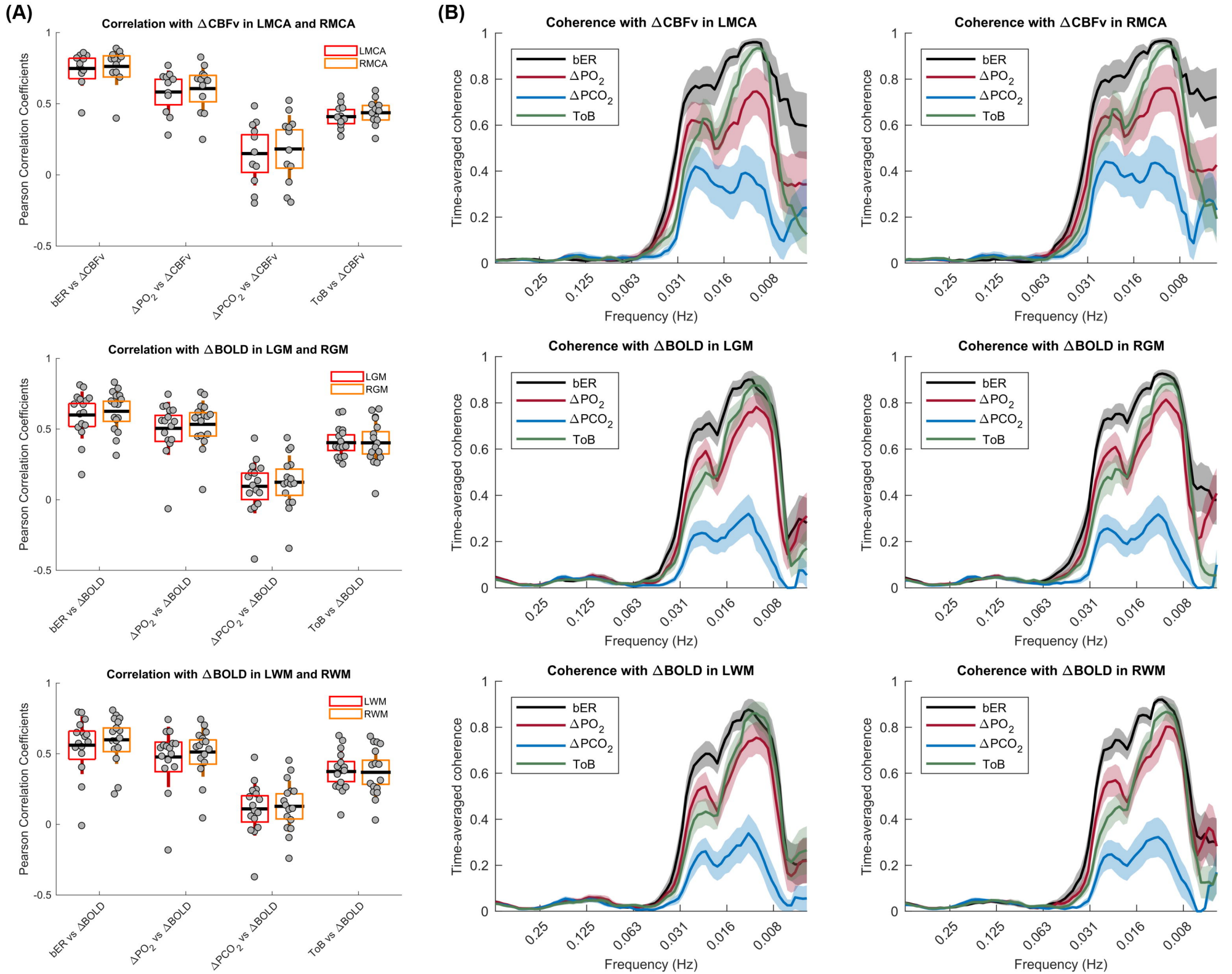
(A)
Correlation with ΔCBFv in LMCA and RMCA
LMCA
RMCA
Pearson Correlation Coefficients
bER vs ΔCBFv
ΔPO2 vs ΔCBFv
ΔPCO2 vs ΔCBFv
ToB vs ΔCBFv
Correlation with ΔBOLD in LGM and RGM
LGM
RGM
bER vs ΔBOLD
ΔPO2 vs ΔBOLD
ΔPCO2 vs ΔBOLD
ToB vs ΔBOLD
Correlation with ΔBOLD in LWM and RWM
LWM
RWM
(B)
Coherence with ΔCBFv in LMCA
Coherence with ΔCBFv in RMCA
Coherence with ΔBOLD in LGM
Coherence with ΔBOLD in RGM
Coherence with ΔBOLD in LWM
Coherence with ΔBOLD in RWM
Time-averaged coherence
bER
ΔPO2
ΔPCO2
ToB
0.25
0.125
0.063
0.031
0.016
0.008
Frequency (Hz)

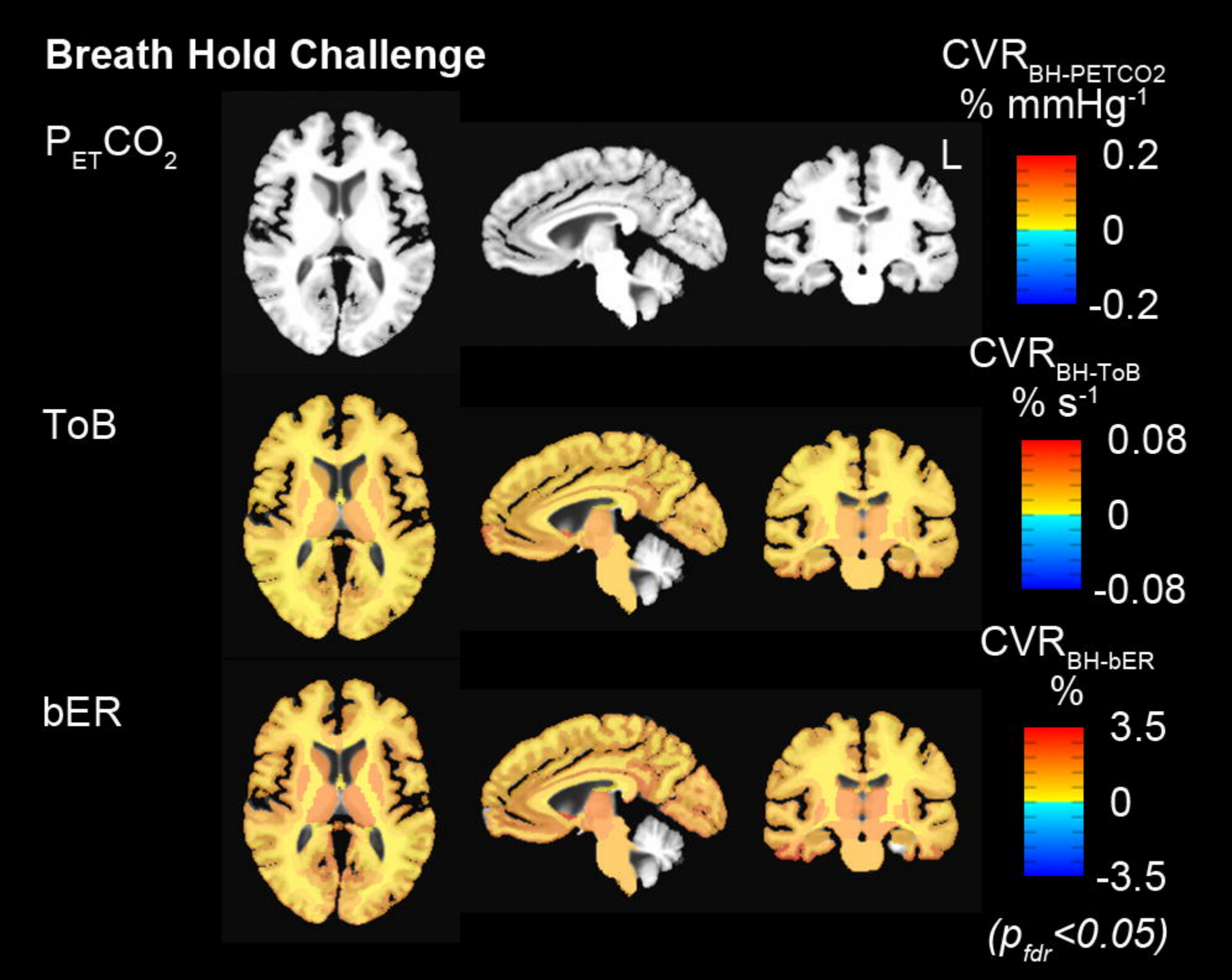
Breath Hold Challenge
$P_{ET}CO_2$
ToB
bER
L
$CVR_{BH\text{-}PETCO2}$
% $mmHg^{-1}$
0.2
0
-0.2
$CVR_{BH\text{-}ToB}$
% s^{-1}
0.08
0
-0.08
$CVR_{BH\text{-}bER}$
%
3.5
0
-3.5
(p_{fdr}<0.05)

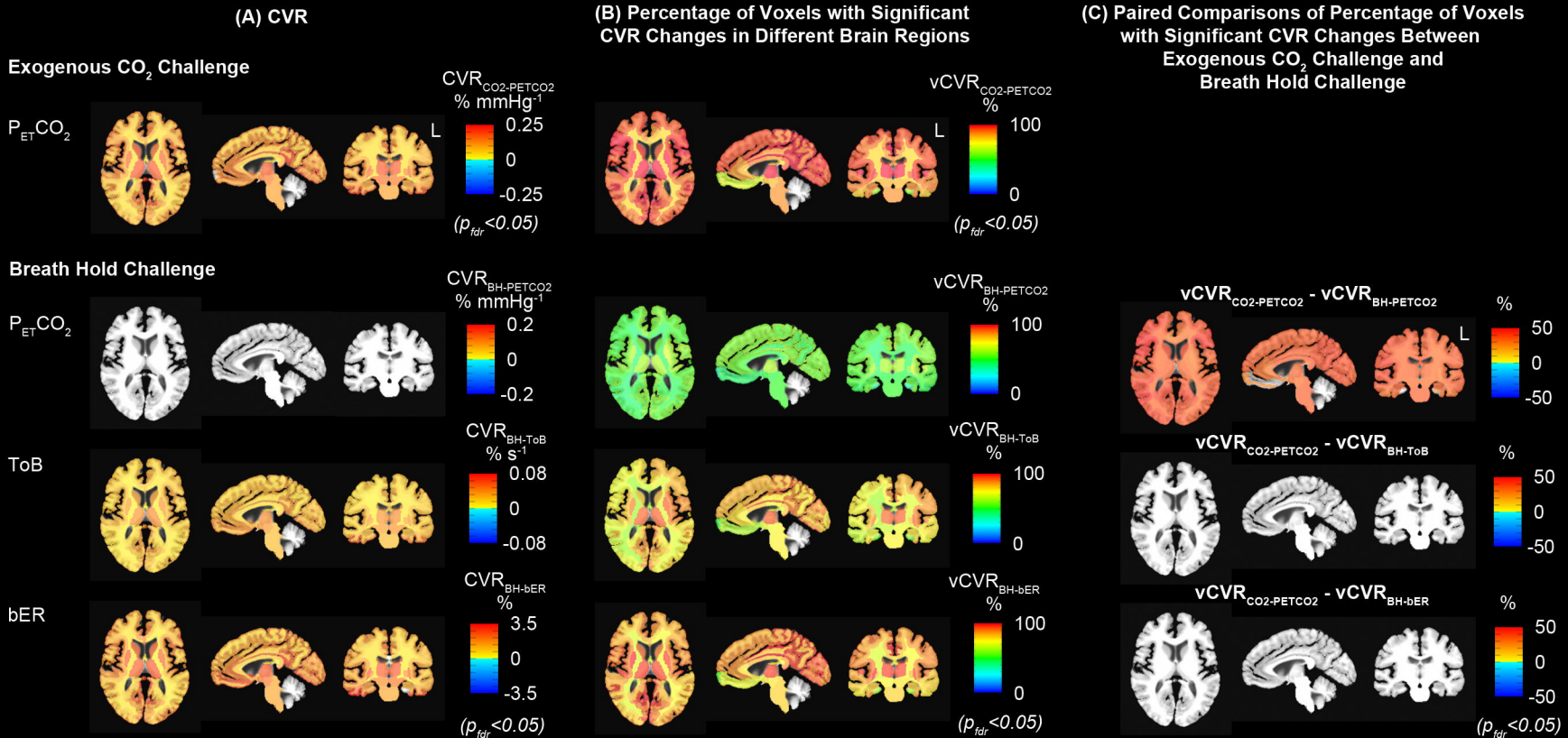
(A) CVR
(B) Percentage of Voxels with Significant CVR Changes in Different Brain Regions
(C) Paired Comparisons of Percentage of Voxels with Significant CVR Changes Between Exogenous CO2 Challenge and Breath Hold Challenge
Exogenous CO2 Challenge
PETCO2
CVRCO2-PETCO2 % mmHg-1
0.25
0
-0.25
(pfdr<0.05)
vCVRCO2-PETCO2 %
100
0
(pfdr<0.05)
Breath Hold Challenge
PETCO2
CVRBH-PETCO2 % mmHg-1
0.2
0
-0.2
vCVRBH-PETCO2 %
100
0
ToB
CVRBH-ToB % s-1
0.08
0
-0.08
vCVRBH-ToB %
100
0
bER
CVRBH-bER %
3.5
0
-3.5
vCVRBH-bER %
100
0
(pfdr<0.05)
vCVRCO2-PETCO2 - vCVRBH-PETCO2 %
50
0
-50
vCVRCO2-PETCO2 - vCVRBH-ToB %
50
0
-50
vCVRCO2-PETCO2 - vCVRBH-bER %
50
0
-50
(pfdr<0.05)
L